إقـــــرار

أنا الموقع أدناه مقدم الرسالة التي تحمل العنوان:

Simulation of Metamaterial Waveguides for Solar Cell Energy by Finite Difference Time Domain Method (FDTD)

أقر بأن ما اشتملت عليه هذه الرسالة إنما هو نتاج جهدي الخاص، باستثناء ما تمت الإشارة إليه حيثما ورد، وإن هذه الرسالة ككل أو أي جزء منها لم يقدم من قبل لنيل درجة أو لقب علمي أو بحثي لدى أي مؤسسة تعليمية أو بحثية أخرى.

DECLARATION

The work provided in this thesis, unless otherwise referenced, is the researcher's own work, and has not been submitted elsewhere for any other degree or qualification

Student's name: اسم الطالب: نادرة صلاح الدين عبد الكريم السلك

Signature: التوقيع: Nadera

Date: التاريخ: 25 - 11 - 2015

The Islamic University of Gaza
Deanery of Higher Studies
Faculty of Science
Department of Physics

Simulation of Metamaterial Waveguides for Solar Cells Energy by Finite Difference Time Domain Method (FDTD)

محاكاة مرشدات موجية لخلايا شمسية تحوي مواد فوق العادة باستخدام طريقة الفرق المحدد المعتمد على الزمن

By
Nadera El-Samak

Supervisor
Prof. Dr. Mohammed Shabat

Submitted to the Faculty of Science as Partial Fulfillment of the Master Degree of Science (M.Sc) in Physics.

2015

بسم الله الرحمن الرحيم

الجامعة الإسلامية – غزة
The Islamic University - Gaza
مكتب نائب الرئيس للبحث العلمي والدراسات العليا هاتف داخلي 1150

الرقم/ج س. غ/35/..... Ref

التاريخ/20/2015/09..... Date

نتيجة الحكم على أطروحة ماجستير

بناءً على موافقة شئون البحث العلمي والدراسات العليا بالجامعة الإسلامية بغزة على تشكيل لجنة الحكم على أطروحة الباحثة/ نادرة صلاح الدين عبد الكريم السمك لنيل درجة الماجستير في كلية العلوم قسم الفيزياء وموضوعها:

محاكاة مرشدات موجية لخلايا شمسية تحوي مواد فوق العادة باستخدام طريقة الفرق المحدد المعتمد على الزمن

Simulation of Metamaterial Waveguides for Solar Cells Energy by Finite Difference Time Domain Method (FDTD)

وبعد المناقشة العلنية التي تمت اليوم الأحد 06 ذو الحجة 1436هـ، الموافق 2015/09/20م الساعة الواحدة ظهراً بمبني طيبة، اجتمعت لجنة الحكم على الأطروحة والمكونة من:

أ.د. محمد موسى شبات	مشرفاً و رئيساً	.....
أ.د. ناصر إسماعيل فرحات	مناقشاً داخلياً	.....
أ.د. علي حامد الأسطل	مناقشاً خارجياً	.....

ويعد المداولة أوصت اللجنة بمنح الباحثة درجة الماجستير في كلية العلوم/ قسم الفيزياء.

واللجنة إذ تمنحها هذه الدرجة فإنها توصيها بتقوى الله ولزوم طاعته وأن تسخر علمها في خدمة دينها ووطنها.

والله ولي التوفيق،،،

نائب الرئيس لشئون البحث العلمي والدراسات العليا

أ.د. عبدالرؤوف علي المناعمة

P.O. Box 108, Rimal, Gaza, Palestine fax: +970 (8) 286 0800 فاكس Tel: +970 (8) 286 0700 هاتف ص.ب. 108 الرمال، غزة، فلسطين
public@iugaza.edu.ps www.iugaza.edu.ps

Abstract

Solar cells provide a renewable and clean energy by converting the sunlight to electricity. However, it is important to reduce the cost of the solar cell and increase the efficiency in order to be considered as a reliable energy source.

In this work, a theoretical analysis for a waveguide structure by using Finite Difference (FD) methods is presented. The fundamental concepts of both Finite Difference Time Domain method (FDTD) and Finite Difference Frequency Domain method (FDFD) are reported in details.

Also, a new waveguide solar cell structure containing metamaterial is presented in order to improve the absorption of light. Metamaterial is an artificial material with negative electric permittivity and negative magnetic permeability which is used to absorb a large amount of the incident light. Finite Difference Time Domain Method is used to analyze the proposed waveguide structure.

We also used MEEP and MATLAB software to run the simulation of the proposed waveguide structure.

الملخص

تتميز الخلايا الشمسية بقدرتها على توفير طاقة متجددة ونظيفة. يعتمد مبدأ عمل الخلايا الشمسية على تحويل الطاقة الضوئية إلى طاقة كهربائية. تواجه الخلايا الشمسية العديد من التحديات منها التكلفة العالية نسبياً عند التصنيع ومدى الفعالية وذلك مقارنة بغيرها من البدائل. مواجهة هذه التحديات مهم جداً لجعل الخلايا الشمسية مصدراً يعتمد عليه للحصول على الطاقة.

في هذه الأطروحة قمنا بدراسة التحليل النظري باستخدام طرق الفرق المحدد. حيث تم إيضاح أساسيات طريقة الفرق المحدد بالاعتماد على الزمن و طريقة الفرق المحدد بالاعتماد على التردد.

قمنا أيضاً بدراسة نموذج لتركيب خلية شمسية يحوي مادة فوق العادة وذلك لتحسين امتصاص الضوء. المادة فوق العادة عبارة عن مادة مصنعة بحيث تكون كل من نفاذيتها الكهربائية وسماحيتها المغناطيسية سالبة. هذه المادة تساعد على امتصاص أكبر قدر ممكن من الضوء الساقط.

كذلك قمنا باستخدام برامج حاسوبية لمحاكاة النموذج المدروس ورسم العلاقات بين المتغيرات المدروسة.

Acknowledgments

I would like to express my gratitude to my advisor, *Prof. Dr. Mohammed Shabat,* for the useful comments, remarks and encouragement through the work of this master thesis.

Furthermore, I would like to thank *Prof. Dr. Xiaoyan Xiong, Dr. Suleiman Baraka, Oussama Enshassi and Raed Rasheed* for their help and cooperation.

Also, I would like to extend my thanks to my dear family for their continuous support.

Special thanks to my loved husband, *Mohammad Al-Afifi*, for his understanding and encouragement.

Table of Contents

List of Figures

List of Abbreviations

SCs	Solar Cells
CIS	Copper-Indium:Diselenide
CIGS	Copper-Indium:Gallium- Diselenide
CdTe	Cadmium Telluride
LHMs	Left Handed Materials
FD	Finite Difference
FDTD	Finite Difference Time Domain
FDFD	Finite Difference Frequency Domain
ABCs	Mur's Absorbing Boundary Conditions
PMLs	Perfect Matched Layers
AR	Antireflection Coating
BR	Back Reflector Coating
SPRs	Surface Plasmon Resonances
PBC	Periodic Boundary Conditions
ADE	Auxiliary Differential Equation
EM	Electromagnetic
SRR	Split Ring Resonator

CHAPTER 1

1. Review of Solar Cell Structure and Materials

1.1 Introduction

Providing enough energy to deal with the increasing demand is one of the greatest world issues. Sustainable energy development is multidimensional case with environmental, economic, social and political aspects. Pollution and lack of energy security are all consequences of using the non-renewable energy sources such as coal, oil, natural gas and uranium. Moreover, the big challenge is the energy availability for future generations. A promising source of energy which would be able to solve a part of the energy crisis for the present and the future is the solar cell. Solar cells provide a renewable and clean energy by converting the sunlight to electricity. However, it is important to reduce the cost of the solar cell and increase the efficiency in order to be a reliable energy source [1].

1.2 Solar Cell Structure

A solar cell is an electrical device that converts the energy of light into electricity by the photovoltaic effect [2, 3]. The photovoltaic effect is the production of current caused by the voltage difference across P-N junction, as a consequence of photons absorption on the top layer of N-type material [4]. The N-type material is usually a shiny effective material in order to send photons bouncing away before they enter the P-junction. An anti-reflective coating is used to limit the reflection of sunlight. There are also finger-like contacts in the top layer which reduce series resistance. The P-type material is layered to a conductive back contact made of aluminum or some alloy. These metal contacts and the fingers on the top electrode are made to facilitate plentiful light to

enter into the N-type and P-type layer and also a pathway for electrical flow out of current. Figure 1.1 shows the basic structure of solar cell.

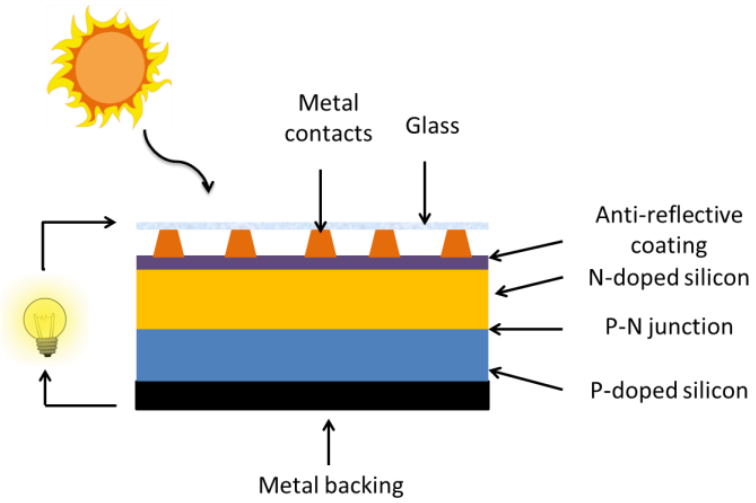

Figure 1.1: Basic structure of a silicon solar cell [5]

1.3 Solar Cell Mechanism

A photon with energy greater than the bandgap energy $(h\nu > E_{gap})$ incident on a semiconductor excites electrons from the valence band to conduction band which allow for a current to flow. The maximum current density is given by the flux of photons with this energy. The excitation of the electron to the conductive band causes a hole in the valence band.

A simple form of a solar cell is a large-area P-N junction. An electron-hole pairs are formed from the energy of the incident light. The electron-hole pairs separate at the junction, with electron (holes) diffusing across the depletion zone to the P-type (N-type) region, where they become thermally free and generate a current [6].

1.4 Limitations of Solar Cells

Regardless of the quality of today's solar cells, the ultimate consumption rate of the best of them today can't exceed the limit of 30% of the sunlight [7]. This can be attributed to the fact that the spectrum of sunlight covers a range of around 0.0012 eV to 4 eV, however, the semi-conductors respond only to part of the sunlight spectrum.

Photons will be able to free electrons and create a current if they have the band gap energy. Meanwhile, if the energy of the photon is less than material's band gap, it passes through the cell without being absorbed causing a waste in incoming energy. Moreover, the surface of the cell always reflects a significant portion of light though the surface which is usually texturized and coated with anti-reflective coating. Furthermore, local recombination of newly created holes and electrons may cause loss of some energy. Finally, some losses of energy are due to manufacturing impurities in solar cells.

Despite these limitations, solar cells do not reduce emissions or any other type of pollution, have no moving parts and require a little maintenance.

1.5 Solar Cell Materials

The current generated from light incident on P-N junction depends on both the mobility of the carriers in material and the exposed surface area of the junction. Thus, semiconductor materials with greater charge mobility and lower cost are needed.

a. **Silicon: Crystalline and Amorphous**

Nowadays, more than 80% of solar cells produced are crystalline silicon solar cells. Where, all of the other 20% are developed as amorphous silicon solar cells.

Commercially, a crystalline silicon solar cell has achieved efficiencies of as much as 16%, while experimentally it has achieved efficiencies of more than 24%. These solar cells have proven to be vigorous in their stability and reliability, even when they are exposed to hard conditions over many years.

However, the use of crystalline silicon has many financial disadvantages. The complex processing procedures and the requirement of large amounts of high purity silicon stock raised the cost of these solar cells. As for the wafer-based cells, the wafer sizes are restricted, and it should be externally assembled and connected to attain a large surface area. Improving the cost and efficiency of wafer-based solar cells can be arranged in either adding an epitaxial layer or dropping amorphous silicon on the wafer surface.

The deposition of a high-quality epitaxial layer with a proper uniformity has provided efficiencies greater than 19%, yet it was hard and costly to implement in the market. However, the deposition of the doped amorphous silicon in order to form a heterojunction has provided similar efficiencies, along with simplifying the processing.

Recently, the interest has been shifted from wafer-based silicon solar cells to thin-films crystalline silicon. The film thickness is less than $10\mu m$. With the addition of hydrogen in the growing crystalline layer, efficient grain-boundary passivation can be attained giving the preferred layer properties with grain size more than $1\mu m$. Meanwhile, the best efficiencies achieved are just below 10%.

In the 1970s, a hydrogenated amorphous silicon (A-Si:H) was presented as a potential material for semiconductor devices. It has become the first thin-film material to enter large-scale production for solar cells. The higher visible spectrum optical absorption over crystalline silicon allows for film thickness much less than $1\mu m$.

A-Si:H solar cells are produced with a P-I-N structure in order to reduce recombination loses. Furthermore, A-Si:H solar cells have only reached an efficiency of 13% in the laboratory and 8% commercially.

Despite being produced by cheaper substrates, A-Si:H has low efficiency and stability issues [1, 8-10].

b. Copper-Indium:Diselenide (CIS) and Copper-Indium:Gallium-Diselenide (CIGS)

Copper-Indium:Diselenide (CIS) and Copper-Indium:Gallium-Diselenide (CIGS) are a direct-gap polycrystalline P-type semiconductors. The minimum of the conduction band and the maximum of the valence band have the same wave vector which leads to achieve a high optical absorption. CIS and CIGS are used in heterojunctions with N-type layers.

In the laboratory, CIS and CIGS have a significantly high efficiency which is about 18.8% for polycrystalline thin-films. The high efficiency is caused by the effective bandgap between 1.1 to 1.2 eV.

CIS and CIGS solar cells offer good stability and reliability, except in considering heat and humidity. While commercial production of these solar cells is

proposed to be significantly cheaper than for wafer-based crystalline silicon solar cells, full scale production will face difficulties with the availability and price of Indium [11].

c. Cadmium Telluride (CdTe)

Cadmium telluride **(**CdTe) is a binary compound. CdTe has a direct bandgap and high optical absorption, but the bandgap energy is about 1.45eV. This causes a higher current densities and higher open-circuit voltage than with CIS/CIGS. Their typical efficiencies are 16% in laboratory and 9% commercially. Another advantage of CdTe solar cells is the significant enhancement of carrier multiplication from CdTe nanocrystals. Carrier multiplication is the process where the inelastic scattering of charge carriers and valence electrons generate additional electron-hole pairs.

However, CdTe is produced from dangerous material (Cd) which introduces dangers that requiring strict regulation [12].

d. Dye-Sensitized

Dye-sensitized photovoltaic solar cells have multilayer structure that separates the process of light absorption and charge carrier transport.

In the laboratory, Dye-sensitized solar cells have achieved an efficiency of about 10%. However, the electrolytic Dye can suffer from stability issues, particularly outside of prescribed temperature range, and additional costs for integrating into series connected system [13].

e. Organic Polymers

Organic materials could be used to produce photovoltaics. However, it was not until the 1990s that conducting organic polymer solar cells were offered an efficiency of 2.9%. Recent researches in laboratory achieved efficiencies as high as 5%.

Organic photovoltaics depend on the illumination of donor and acceptor species. This illumination causes the separation of excitons, much like in inorganic semiconductors. Organic solar cells are constructed out of several organic polymers, usually embedded with fullerene which is acting as acceptor.

However, the performance of the organic solar cells suffers from several issues. One of these issues is the correlation between the separation of the bound electron-hole exciton, which is the primary difference between organic and inorganic solar cells. Excitons experience stronger correlation in organic polymers. The bound state formed by the electron-hole pair gives the charge separation a particularity in efficiencies. Furthermore, recent researches work on the construction of these polymers in order to increase the light absorption in the spectrum of visible light, and also to deal with nonlinear optical properties.

Even with its infancy and low efficiencies, organic solar cells propose a very attractive alternative to inorganic thin-films. Using the organic polymers reduces the production cost of solar cells and that is beside the advantage of being lightweight and flexible [14, 15].

f. Nano-Scale Materials

Nanocrystals can be used as an effective and inexpensive solar cell. Controlling the size and shape of nanocrystals allows the customization of bandgap through absorption of light across the whole spectrum. The three dimension confinement achieves greater impact ionization and results in multiple charge carrier creation from a single photon. The confinement raises the density of states along the band edge in a given dimension. With this property, and control of the inter-crystal spacing, the nanocrystals can act as artificial atoms that allow for tuning of discrete electronic states via size regulation [16, 17].

g. **Metamaterial**

In electromagnetic theory, electric permittivity $\boldsymbol{\varepsilon}$ and magnetic permeability $\boldsymbol{\mu}$ are the most important parameters to characterize the electromagnetic property of a medium. The permittivity describes how an electric field affects, and is affected by the medium. Whereas, the permeability describes how a magnetic field affects, and is affected by the medium. And all this is determined by the ability of a material to polarize in response to the electric and magnetic field, respectively [18]. Figure 1.2 shows the material parameter space characterized by electric permittivity and magnetic permeability.

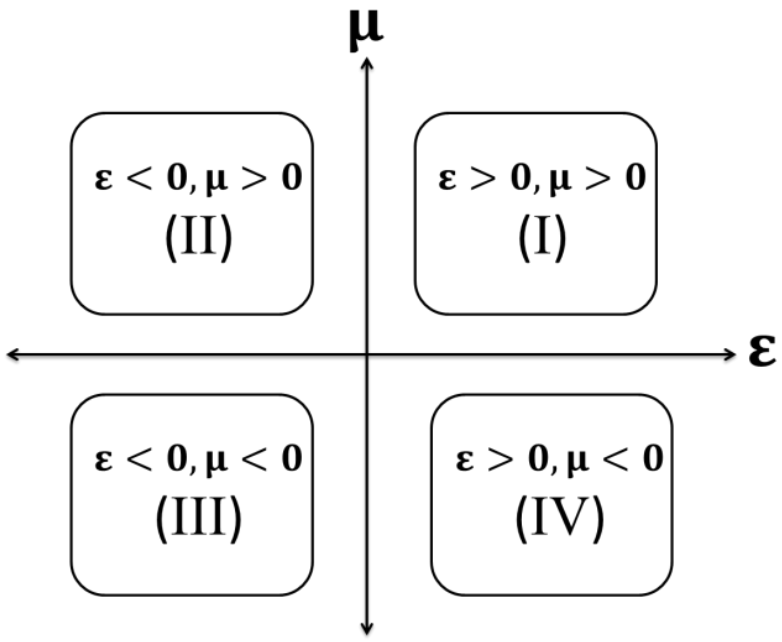

Figure 1.2: Material parameter space characterized by electric permittivity (ε) and magnetic permeability (μ).

Region (I) in the upper right quadrant employs material with simultaneously positive permittivity and permeability, which include most dielectric materials. Region (II) comprises of metals, ferroelectric materials, and doped semiconductors which is able to exhibit negative permittivity at certain frequencies. Region (IV) embraces some ferrite materials with negative permeability. Region (III) involves material with both negative permittivity and permeability. So, this material is called double-negative material due to its double negative values of permittivity and permeability. In this material, the directions of the electric field (**E**), the magnetic field (**H**)**,** and the wave propagation vector (**K**) obey the left-hand rule instead of the right-hand rule in ordinary dielectric materials, so it can be called left-handed materials (LHMs). Moreover, when the electromagnetic waves propagate on this material, the refraction is reversed. So, they are also called negative index material. Furthermore, this material can exhibit properties not found in nature, so it called a metamaterial. Where, the prefix "meta" means "altered" or "beyond" [19], that is metamaterials can have their electromagnetic properties altered to something beyond what had been found in nature.

- **Brief History of Metamaterial**

In 1968, Victor Veselago theoretically analyzed the propagation of plane wave in a material with both negative permittivity $\boldsymbol{\varepsilon}$ and negative permeability $\boldsymbol{\mu}$, and that was the first study in this field [20].

Pendry et al.[21, 22] suggested and then experimentally proved that a composite medium of periodically placed thin metallic wires can act as an effective plasma medium for radiation with wavelength much larger than the spatial periodicity of the structure. For frequencies lower than a particular (plasma) frequency, the thin wire structure therefore displays a negative permittivity $\boldsymbol{\varepsilon}$.

Smith et al.[23] constructed a metamaterial using the combination of periodic rods and split rings. They implemented many experiments in microwave range to emphasize its phenomenal prosperities.

In 2001, Shelby et al[24] were attained the first experimental investigation of negative index of refraction.

Kong [25] studied the interaction of electromagnetic waves with stratified isotropic metamaterials. He scrutinized the field solution of guided waves, the reflection and transmission beams, and linear and dipole antennas in stratified structure of metamaterials.

In 2003, Engheta [26] demonstrated the theory of metamaterials and their electromagnetic properties, possible future applications and physical remarks.

Chew [27] had analyzed the metamaterial energy conservation property and the realistic Sommerfeld Problem of a point source over a metamaterial half space and a metamaterial slab. In 2006, Sabah et al[28] presented the reflected and transmitted powers resulted from the interaction of electromagnetic waves with a metamaterial. They studied the effects of the structure parameter, incidence angle, and the frequency on the reflected and transmitted powers for lossless metamaterial. The electromagnetic wave propagation though frequency dispersive and lossy double negative slab embedded between two different semi-infinite media was introduced by Sabah et al[29].

- **Theoretical Aspects**

Maxwell's Equations can be used to characterize metamaterial. In order to describe metamaterial, a transformation of Maxwell's Equations need to be considered.

Consider a plane wave propagates in an isotropic, homogenous medium. The electric field is

$$\mathbf{E}(\omega, \mathbf{k}) = \mathbf{E}_0 \exp j(\mathbf{k}.\mathbf{r} - \omega.t) \tag{1.1}$$

and the magnetic field is

$$\mathbf{H}(\omega, \mathbf{k}) = \mathbf{H}_0 \exp j(\mathbf{k}.\mathbf{r} - \omega.t) \quad (1.2)$$

In case of a free charges space, Maxwell's Equations in the time domain:

$$\boldsymbol{\nabla}.\mathbf{B} = 0 \quad (1.3)$$

$$\boldsymbol{\nabla} \times \mathbf{E} = -\frac{\partial \mathbf{B}}{\partial \mathrm{t}} \quad (1.4)$$

$$\boldsymbol{\nabla}.\mathbf{D} = 0 \quad (1.5)$$

$$\nabla \times \mathbf{H} = \frac{\partial \mathbf{D}}{\partial \mathrm{t}} \quad (1.6)$$

and constitutive equations are

$$\mathbf{D} = \varepsilon \mathbf{E} = \varepsilon_0 \varepsilon_r \mathbf{E} \quad (1.7)$$

$$\mathbf{B} = \mu \mathbf{H} = \mu_0 \mu_r \mathbf{E} \quad (1.8)$$

can be simplified into

$$\mathbf{k} \times \mathbf{E} = \mu\omega\mathbf{H} \quad (1.9)$$

$$\mathbf{k} \times \mathbf{H} = -\varepsilon\omega\mathbf{E} \quad (1.10)$$

where, **D** is the electric induction, **B** is the magnetic induction, ε_0 is the permittivity of vacuum, μ_0 is the permeability of vacuum, ε_r is the permittivity of the medium and μ_r is the permeability of the medium.

Since the permittivity and permeability are both negative, Eq. (1.9) and Eq. (1.10) change to,

$$\mathbf{k} \times \mathbf{E} = -\mu\omega\mathbf{H} \quad (1.11)$$

$$\mathbf{k} \times \mathbf{H} = \varepsilon\omega\mathbf{E} \quad (1.12)$$

Metamaterial properties come from its structure rather than from its composition. Metamaterials consist of periodically distributed structured elements, where the size and space of these elements are much smaller than the wavelength of the Electromagnetic (EM) waves. As a consequence, the microscopic detail of each individual structure cannot be affected by EM waves. These collective of inhomogeneous objects can be characterized by an equivalent homogenous material with effective relative permittivity ($\varepsilon_{\mathrm{r,eff}}$) and permeability

($\mu_{r,eff}$) at the macroscopic level. Moreover, the effective relative permittivity and permeability obey the Drude-Lorentz model [18] as

$$\varepsilon_{r,eff}(\omega) = 1 - \frac{\omega_{p,eff}^2}{\omega(\omega + j\gamma_{eff})} \tag{1.13}$$

$$\mu_{r,eff}(\omega) = 1 - \frac{F\omega^2}{\omega^2 - \omega_0^2 + j\Gamma\omega} \tag{1.14}$$

where, $\omega_{p,eff}$ is the effective plasma frequency, ω_0 is the resonance frequency, γ_{eff} is the damping factor, F is the filling ratio of the Split Ring Resonator (SRR), and Γ is the damping term.

The advantage of metamaterial is that both the permittivity ($\varepsilon_{r,eff}$) and permeability ($\mu_{r,eff}$) can be controlled using an accurately designed structures.

All the above mentioned are leading to find out the possibilities of design and manufacture of a new solar cell waveguide.

CHAPTER 2

2. Finite Difference Approach

2.1 Introduction

Modeling and numerical simulation have grown increasingly as a tool for understanding and analyzing any problem in science. The Finite Difference approximations for derivative are one of the simplest methods to solve differential equation. The beginning of Finite Difference method in numerical application was in early 1950s [30] . Since then, many modifications were made on this application.

2.2 Finite Difference

Finite-Difference methods approximate the solutions of differential equations by replacing derivative expressions with approximately equivalent difference quotients [30-32]. First, we examine the finite difference approximations for derivatives and then examine the accuracy of these approximations.

Consider a continuous and smooth one dimensional function $f(x)$,with

$$f_1 = f(-h_1) \tag{2.1}$$

$$f_2 = f(h_2) \tag{2.2}$$

$$f_3 = f(0) \tag{2.3}$$

Now, we can write f_1 and f_2 as Taylor series expansions around x=0 as

$$f_1 = f(-h_1) = f(0) - \frac{1}{1!}h_1 f^{(1)}(0) + \frac{1}{2!}h_1^2 f^{(2)}(0) - \frac{1}{3!}h_1^3 f^{(3)}(0) + \mathcal{O}(h_1^4) \tag{2.4}$$

$$f_2 = f(h_2) = f(0) - \frac{1}{1!}h_2 f^{(1)}(0) + \frac{1}{2!}h_2^2 f^{(2)}(0) - \frac{1}{3!}h_2^3 f^{(3)}(0) + \mathcal{O}(h_2^4) \tag{2.5}$$

where, $f^{(n)}$ is the nth derivative defined as

$$f^{(n)}(x) = \frac{d^n f(x)}{dx^n} \tag{2.6}$$

Subtracting Eq. (2.4) from Eq. (2.5), we get an expression for the first derivative

$$f_2 - f_1 = (h_2 + h_1)f^{(1)}(0) + \frac{1}{2}(h_2^2 - h_1^2)f^{(2)}(0) + \mathcal{O}(h^3) \tag{2.7}$$

thus,

$$f^{(1)}(0) = \frac{f_2 - f_1}{h_2 + h_1} + \frac{1}{2}(h_2 - h_1)f^{(2)}(0) + \mathcal{O}(h^2) \tag{2.8}$$

From Eq. (2.8), the error caused by approximating the first derivative at x = 0 with the differential expression

$$f^{(1)}(0) = \frac{f_2 - f_1}{h_2 + h_1} \tag{2.9}$$

is $\mathcal{O}(h^2)$ when $h_1 = h_2$ and is $\mathcal{O}(h)$ when $h_1 \neq h_2$

The error caused by approximating the second derivative with the expression

$$f^{(2)}(0) = \frac{2}{h_1 h_2}\frac{h_2 f_1 - (h_1 + h_2)f_3 + h_1 f_2}{(h_1 + h_2)} \tag{2.10}$$

is $\mathcal{O}(h^2)$ when $h_1 = h_2$ and is $\mathcal{O}(h)$ when $h_1 \neq h_2$.

From the above discussion, we can conclude that the error reflects the fact that a finite part of Taylor series is used in the approximation.

2.3 Finite Difference Time Domain (FDTD)

The Finite Difference Time Domain (FDTD) is one of the most effective numerical methods in the study of waveguides [33, 34]. As a direct solution to the Maxwell's Equations, FDTD method offers a simple way to model the complex periodic structures.

FDTD method is based on numerically solution of Maxwell's curl equations. In this method, the time and space derivatives are approximated using finite difference approximations. While the **E** and **H** fields are evaluated iteratively at alternative half-time steps.

2.3.1 The Yee Algorithm

The FDTD algorithm was first proposed by Kane Yee in 1966, and then improved by others in early 70s [35]. The algorithm describes the basics of the FDTD model to solve

Maxwell's curl equations in time domain. First, we replace all the derivatives in Ampere's and Faraday's Laws with finite differences and then discretize space and time to keep the electric and magnetic fields staggered in both space and time. Next step is to solve the resulting difference equations to obtain the update equations that express the unknown future fields in terms of known previous fields. Thus, we can evaluate the magnetic fields and then electric fields one time-step into the future. Now, we need to repeat the previous two steps until the fields have been obtained over the desired duration.

Yee used a special grid cell which called Yee cell and it discretizes the three dimensional space into cubes. Figure 2.1 shows the unit cell of Yee lattice. As can be seen from the figure, the electric fields are along the edges of the cube while the magnetic fields are located at the center of the cube's six surfaces. Each unit cell has twelve magnetic fields and six electric fields. Since each electric field is shared by the adjacent four unit cells, each unit cell possesses three electric fields, namely E_x, E_y and E_z. Similar rule applies to magnetic fields and each unit cell possesses three magnetic fields, $H_x, H_y$and H_z. In a three dimension point of view, each magnetic field H is surrounded by four circulating electric field E fields, which interprets the Ampere's Law. Similarly, every electric field E is surrounded by four circulating magnetic field H fields, representing the Faraday's Law.

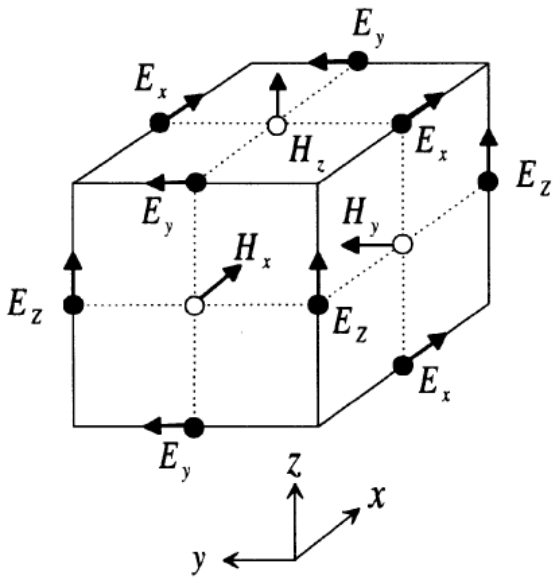

Figure 2.1: The unit cell of Yee lattice

2.3.2 Discretization of Electromagnetic Waves

The time-dependent Maxwell's curl equations are

$$-\mu \frac{\partial \boldsymbol{H}}{\partial t} = \boldsymbol{\nabla} \times \boldsymbol{E} \tag{2.11}$$

$$\varepsilon \frac{\partial \boldsymbol{E}}{\partial t} = \boldsymbol{\nabla} \times \boldsymbol{H} \tag{2.12}$$

In the three-dimensional case, Eq. (2.11) and Eq. (2.12) can be converted into three scalar equations, forming six scalar equations in total

$$-\mu \frac{\partial H_x}{\partial t} = \frac{\partial E_z}{\partial y} - \frac{\partial E_y}{\partial z} \tag{2.13}$$

$$-\mu \frac{\partial H_y}{\partial t} = \frac{\partial E_x}{\partial z} - \frac{\partial E_z}{\partial x} \tag{2.14}$$

$$-\mu \frac{\partial H_z}{\partial t} = \frac{\partial E_y}{\partial x} - \frac{\partial E_x}{\partial y} \tag{2.15}$$

$$\varepsilon \frac{\partial E_x}{\partial t} = \frac{\partial H_z}{\partial y} - \frac{\partial H_y}{\partial z} \tag{2.16}$$

$$\varepsilon \frac{\partial E_y}{\partial t} = \frac{\partial H_x}{\partial z} - \frac{\partial H_z}{\partial x} \tag{2.17}$$

$$\varepsilon \frac{\partial E_z}{\partial t} = \frac{\partial H_y}{\partial x} - \frac{\partial H_x}{\partial y} \tag{2.18}$$

For a function **F** of space and time, it can be discretized as

$$f(x, y, z, t) = f(i\Delta x, j\Delta y, k\Delta z, n\Delta t) = f^n(i, j, k) \tag{2.19}$$

where, $\Delta x, \Delta y$ and Δz are the space discretization, and Δt is the time step. Now, using the central difference approximation

$$\frac{\partial f(x, y, z, t)}{\partial x} \approx \frac{f^n\left(i + \frac{1}{2}, j, k\right) - f^n\left(i - \frac{1}{2}, j, k\right)}{\Delta x} \tag{2.20}$$

$$\frac{\partial f(x, y, z, t)}{\partial y} \approx \frac{f^n\left(i, j + \frac{1}{2}, k\right) - f^n\left(i, j - \frac{1}{2}, k\right)}{\Delta y} \tag{2.21}$$

$$\frac{\partial f(x, y, z, t)}{\partial z} \approx \frac{f^n\left(i, j, k + \frac{1}{2}\right) - f^n\left(i, j, k - \frac{1}{2}\right)}{\Delta z} \tag{2.22}$$

$$\frac{\partial f(x, y, z, t)}{\partial t} \approx \frac{f^{n+\frac{1}{2}}(i, j, k) - f^{n-\frac{1}{2}}(i, j, k)}{\Delta t} \tag{2.23}$$

The three dimension finite difference time domain expressions for the Eqs. (2.13)- (2.18) respectively are

$$\begin{aligned} H_x^{n+\frac{1}{2}}\left(i, j + \frac{1}{2}, k + \frac{1}{2}\right) &= H_x^{n-\frac{1}{2}}\left(i, j + \frac{1}{2}, k + \frac{1}{2}\right) \\ &- \frac{\Delta t}{\mu \Delta y}\left[E_z^n\left(i, j + 1, k + \frac{1}{2}\right) - E_z^n\left(i, j, k + \frac{1}{2}\right)\right] \\ &+ \frac{\Delta t}{\mu \Delta z}\left[E_y^n\left(i, j + \frac{1}{2}, k + 1\right) - E_y^n(i, j + \frac{1}{2}, k)\right] \end{aligned} \tag{2.24}$$

$$\begin{aligned} H_y^{n+\frac{1}{2}}\left(i + \frac{1}{2}, j, k + \frac{1}{2}\right) &= H_y^{n-\frac{1}{2}}\left(i + \frac{1}{2}, j, k + \frac{1}{2}\right) \\ &- \frac{\Delta t}{\mu \Delta z}\left[E_x^n\left(i + \frac{1}{2}, j, k + 1\right) - E_x^n\left(i + \frac{1}{2}, j, k\right)\right] \\ &+ \frac{\Delta t}{\mu \Delta x}\left[E_z^n\left(i + 1, j, k + \frac{1}{2}\right) - E_z^n(i, j, k + \frac{1}{2})\right] \end{aligned} \tag{2.25}$$

$$
\begin{aligned}
H_z^{n+\frac{1}{2}}\left(i+\frac{1}{2},j+\frac{1}{2},k\right) &\\
&= H_z^{n-\frac{1}{2}}\left(i+\frac{1}{2},j+\frac{1}{2},k\right)\\
&-\frac{\Delta t}{\mu\Delta x}\left[E_y^n\left(i+1,j+\frac{1}{2},k\right)-E_y^n\left(i,j+\frac{1}{2},k\right)\right]\\
&+\frac{\Delta t}{\mu\Delta y}\left[E_x^n\left(i+\frac{1}{2},j+1,k\right)-E_x^n(i+\frac{1}{2},j,k)\right]
\end{aligned}
\tag{2.26}
$$

$$
\begin{aligned}
E_x^{n+1}\left(i+\frac{1}{2},j,k\right) &\\
&= E_x^n\left(i+\frac{1}{2},j,k\right)\\
&+\frac{\Delta t}{\varepsilon\Delta y}\left[H_z^{n+\frac{1}{2}}\left(i+\frac{1}{2},j+\frac{1}{2},k\right)-H_z^{n+\frac{1}{2}}\left(i+\frac{1}{2},j-\frac{1}{2},k\right)\right]\\
&-\frac{\Delta t}{\varepsilon\Delta z}\left[H_y^{n+\frac{1}{2}}\left(i+\frac{1}{2},j,k+\frac{1}{2}\right)-H_y^{n+\frac{1}{2}}(i+\frac{1}{2},j,k-\frac{1}{2})\right]
\end{aligned}
\tag{2.27}
$$

$$
\begin{aligned}
E_y^{n+1}\left(i,j+\frac{1}{2},k\right) &\\
&= E_y^n\left(i,j+\frac{1}{2},k\right)\\
&+\frac{\Delta t}{\varepsilon\Delta z}\left[H_x^{n+\frac{1}{2}}\left(i,j+\frac{1}{2},k+\frac{1}{2}\right)-H_x^{n+\frac{1}{2}}\left(i,j+\frac{1}{2},k-\frac{1}{2}\right)\right]\\
&-\frac{\Delta t}{\varepsilon\Delta x}\left[H_z^{n+\frac{1}{2}}\left(i+\frac{1}{2},j+\frac{1}{2},k\right)-H_z^{n+\frac{1}{2}}(i-\frac{1}{2},j+\frac{1}{2},k)\right]
\end{aligned}
\tag{2.28}
$$

$$
\begin{aligned}
E_z^{n+1}\left(i,j,k+\frac{1}{2}\right) &= E_z^n\left(i,j,k+\frac{1}{2}\right)\\
&+\frac{\Delta t}{\varepsilon\Delta x}\left[H_y^{n+\frac{1}{2}}\left(i+\frac{1}{2},j,k+\frac{1}{2}\right)-H_y^{n+\frac{1}{2}}\left(i-\frac{1}{2},j,k+\frac{1}{2}\right)\right]\\
&-\frac{\Delta t}{\varepsilon\Delta y}\left[H_x^{n+\frac{1}{2}}\left(i,j+\frac{1}{2},k+\frac{1}{2}\right)-H_x^{n+\frac{1}{2}}(i,j-\frac{1}{2},k+\frac{1}{2})\right]
\end{aligned}
\tag{2.29}
$$

2.3.3 Boundary Conditions

In numerical modeling, it's not possible to handle an open region problem directly since the data storage in a computer is limited by the size of memory. To solve this problem, an Absorbing Boundary Conditions (ABCs) is used to limit the computational domain.

The ABCs can be divided into two different categories, the first one derived from differential equations and the second one is based on the use of absorbing material.

The most widely used ABCs in the first category is the one derived by Engquist and Majda with discretization given by Mur [36, 37]. It is based on an approximation of the outgoing wave equation being expressed using a Taylor approximation.

The material-based ABCs are realized by surrounding the computational domain with a lossy material that dampens the outgoing fields.

Here, we discuss Mur's second-order ABC and Berenger's Perfect Matched layers (PMLs).

a. Mur's Absorbing Boundary Conditions (ABCs)

Engquist and Majda derived a theory for one-way wave equations that describes wave propagation only in specified directions. For example, consider the two-dimensional wave equation in Cartesian coordinates

$$\frac{\partial^2 U}{\partial x^2}+\frac{\partial^2 U}{\partial y^2}-\frac{1}{c^2}\frac{\partial^2 y}{\partial t^2}=0 \tag{2.30}$$

where, U is a scalar field component and c is the phase velocity of the wave.

We define the partial differential operator as

$$L=\frac{\partial^2}{\partial x^2}+\frac{\partial^2}{\partial y^2}-\frac{1}{c^2}\frac{\partial^2}{\partial t^2}=D_x^2+D_y^2+\frac{1}{c^2}D_t^2 \tag{2.31}$$

Using operator L to write the wave equation

$$LU=L^+L^-U=0 \tag{2.32}$$

where, L^- and L^+ are the factors of the wave operator L, defined as

$$L^-=D_x-\frac{D_t}{c}\sqrt{1-s^2} \tag{2.33}$$

and

$$L^+=D_x+\frac{D_t}{c}\sqrt{1-s^2} \tag{2.34}$$

where,

$$s=\frac{D_y}{D_t/c} \tag{2.35}$$

Using the Second-Order Taylor Series Expansion to approximate the square-root function in Eqs. (2.33) and (2.34), we have

$$\sqrt{1-s^2}\cong 1-\frac{1}{2}s^2 \tag{2.36}$$

Substituting Eq. (2. 36) into Eq. (2.33) and Eq. (2.34), we obtain

$$L^{+} \approx D_x + \frac{D_t}{c}\left[1 - \frac{1}{2}\left(\frac{cD_y}{D_t}\right)^2\right] = D_x - \frac{D_t}{c} + \frac{cD_y^2}{2D_t} \tag{2.37}$$

$$L^{-} \approx D_x - \frac{D_t}{c}\left[1 - \frac{1}{2}\left(\frac{cD_y}{D_t}\right)^2\right] = D_x + \frac{D_t}{c} + \frac{cD_y^2}{2D_t} \tag{2.38}$$

Now, substituting Eq. (2.38) into Eq. (2.32)

$$\left(D_x + \frac{D_t}{c} + \frac{cD_y^2}{2D_t}\right)\left(D_x - \frac{D_t}{c} + \frac{cD_y^2}{2D_t}\right) U = 0 \tag{2.39}$$

Multiplying by D_t

$$\left(D_x D_t + \frac{D_t^2}{c} + \frac{cD_y^2}{2D_t^2}\right)\left(D_x D_t - \frac{D_t^2}{c} + \frac{cD_y^2}{2D_t^2}\right) U = 0 \tag{2.40}$$

Mur used a simple central-difference scheme in the Yee's space with spatial increments Δx and Δy and the time with time step Δt domain.

$$\frac{\partial^2 U|_{\frac{1}{2},j}^{n}}{\partial x \partial t} = \frac{1}{2\Delta t}\left[\left(\frac{U|_{1,j}^{n+1} - U|_{0,j}^{n+1}}{\Delta x}\right) - \left(\frac{U|_{1,j}^{n-1} - U|_{0,j}^{n-1}}{\Delta x}\right)\right] \tag{2.41}$$

The discretized version of the tangential field under discretization at the boundary is calculated as follows

$$\begin{aligned} U|_{0,j}^{n+1} = & -U|_{1,j}^{n-1} + \frac{c\Delta t - \Delta}{c\Delta t + \Delta}\left(U|_{1,j}^{n+1} + U|_{0,j}^{n-1}\right) \\ & + \frac{2\Delta}{c\Delta t + \Delta}\left(U|_{1,j}^{n} + U|_{0,j}^{n}\right) \\ & + \frac{(c\Delta t)^2}{2\Delta(c\Delta t + \Delta)}\left(U|_{0,j+1}^{n} - 2U|_{0,j}^{n} + U|_{0,j-1}^{n}\right) \\ & + \frac{(c\Delta t)^2}{2\Delta(c\Delta t + \Delta)}\left(U|_{1,j+1}^{n} - 2U|_{1,j}^{n} + U|_{1,j-1}^{n}\right) \end{aligned} \tag{2.42}$$

Assuming $\Delta x = \Delta y = \Delta$. Eq. (2.42) represents a Second-Order Mur ABC at the boundary $x = 0$.

The disadvantage of using the Second-Order Mur condition is in addition to use the previous field values at time step (n), prior values at time step (n-1) are required and thus must be stored in memory during the simulation.

b. **Perfect Matched Layers (PMLs)**

The PML is typically pertinent to the continuous world. In continuous world the PML should indeed work perfectly for all incident angles and for all frequencies. There are different PML formulations. All PML's act as a lossy material which is used to absorb the fields traveling away from the interior of the grid.

The PML was originally proposed by Berenger in 1994 [38, 39]. He splits each field component into two parts to create anisotropic (non-physical) medium with the required phase velocity and conductivity to eliminate reflections at an interface between a PML and non-PML region. The actual field components were the sum of these two parts. Since Berenger first paper, others have described PML's using different approaches as Chew et al[40].

Using the Cartesian Coordinate, the six field components yield twelve subcomponents, denoted by $E_{xy}, E_{xz}, E_{yx}, E_{yz},, E_{zx}, E_{zy}, H_{xy}, H_{xz}, H_{yx}, H_{yz}, H_{zx}$ and H_{zy}. To get the actual field, we sum these components, for example

$$E_z = E_{zx} + E_{zy} \tag{2.43}$$

Now using these components, Maxwell's equations can be replaced by the following twelve equations,

$$\varepsilon \frac{\partial E_{xy}}{\partial t} + \sigma_y E_{xy} = \frac{\partial \left(H_{zx} + H_{zy}\right)}{\partial y} \tag{2.44}$$

$$\varepsilon \frac{\partial E_{xz}}{\partial t} + \sigma_z E_{xz} = -\frac{\partial \left(H_{yz} + H_{yx}\right)}{\partial z} \tag{2.45}$$

$$\varepsilon \frac{\partial E_{yz}}{\partial t} + \sigma_z E_{yz} = \frac{\partial \left(H_{xy} + H_{xz}\right)}{\partial z} \tag{2.46}$$

$$\varepsilon \frac{\partial E_{yx}}{\partial t} + \sigma_x E_{yx} = -\frac{\partial \left(H_{zx} + H_{zy}\right)}{\partial x} \tag{2.47}$$

$$\varepsilon \frac{\partial E_{zx}}{\partial t} + \sigma_x E_{zx} = \frac{\partial \left(H_{yz} + H_{yx}\right)}{\partial x} \tag{2.48}$$

$$\varepsilon \frac{\partial E_{zy}}{\partial t} + \sigma_y E_{zy} = -\frac{\partial \left(H_{xy} + H_{xz}\right)}{\partial y} \tag{2.49}$$

$$\mu \frac{\partial H_{xy}}{\partial t} + \sigma_y^* H_{xy} = -\frac{\partial \left(E_{zx} + E_{zy}\right)}{\partial y} \tag{2.50}$$

$$\mu\frac{\partial H_{xz}}{\partial t}+\sigma_z^* H_{xz}=\frac{\partial\left(E_{yz}+E_{yx}\right)}{\partial z} \tag{2.51}$$

$$\mu\frac{\partial H_{yz}}{\partial t}+\sigma_z^* H_{yz}=-\frac{\partial\left(E_{xy}+E_{xz}\right)}{\partial z} \tag{2.52}$$

$$\mu\frac{\partial H_{yx}}{\partial t}+\sigma_x^* H_{yx}=\frac{\partial\left(E_{zx}+E_{zy}\right)}{\partial x} \tag{2.53}$$

$$\mu\frac{\partial H_{zx}}{\partial t}+\sigma_x^* H_{zx}=-\frac{\partial\left(E_{yz}+E_{yx}\right)}{\partial x} \tag{2.54}$$

$$\mu\frac{\partial H_{zy}}{\partial t}+\sigma_y^* H_{zy}=\frac{\partial\left(E_{xy}+E_{xz}\right)}{\partial y} \tag{2.55}$$

where, the parameters $\left(\sigma_x, \sigma_y, \sigma_z, \sigma_x^*, \sigma_y^*, \sigma_z^*\right)$ are homogeneous electric and magnetic conductivities.

Applying the central difference approximation to the temporal and spatial partial differential operator in order to get the relevant FDTD equations incorporating the PML absorbing boundary conditions. For example, Eq. (2.44) becomes

$$\begin{aligned} E_{xy}^{n+\frac{1}{2}}(i,j,k) = & \frac{\frac{1}{\Delta t}-\frac{\sigma_y}{2\varepsilon}}{\frac{1}{\Delta t}+\frac{\sigma_y}{2\varepsilon}} E_{xy}^{n-\frac{1}{2}}(i,j,k) \\ & + \frac{1}{\left(\frac{1}{\Delta t}+\frac{\sigma_y}{2\varepsilon}\right).\varepsilon\Delta y}\left[H_{zx}^n(i,j+1,k)\right. \\ & \left. - H_{zx}^n(i,j,k) + H_{zy}^n(i,j+1,k) - H_{zy}^n(i,j,k)\right] \end{aligned} \tag{2.56}$$

The PMLs is an isotropic and constructed in such a way without any loss in the direction tangential to the interface between the lossless region and the PMLs. However, in the PMLs there is always loss in the direction normal to the interface.

The PML scheme suppresses reflections better than Mur's ABC does. However, Mur's condition is easier to use.

2.3.4 Stability Conditions

In FDTD method, the choice of space increment Δx and the time step Δt can affect the velocity of propagation of numerical waves in finite difference grid approximation, and therefore the numerical error. Here, the stability conditions using the one dimensional scalar Helmhotz equation will be discussed.

$$\frac{\partial^2 U}{\partial x^2} - \varepsilon\mu \frac{\partial^2 U}{\partial t^2} = 0 \tag{2.57}$$

where, $\boldsymbol{U}$ is the one dimension wave function that designates the time-dependent field. Using β_x as the x-directed propagation constant, we express this wave function as

$$U(x,t) = \exp(j\beta_x x)\exp(\alpha t) \tag{2.58}$$

$$U(x,t) = \exp(j\beta_x p\Delta x)\exp(\alpha n\Delta t) \tag{2.59}$$

$$U(x,t) = \exp(j\beta_x p\Delta x)\,\xi^n \tag{2.60}$$

where, $\xi^n = \exp(\alpha n\Delta t)$.

Now, if the field $\boldsymbol{U}$ is stable, ξ must satisfy the condition

$$|\xi| \le 1 \tag{2.61}$$

Substituting Eq. (2.60) into Eq. (2.57), we get

$$\begin{aligned} &\frac{1}{(\Delta x)^2}\{exp[j\beta_x(p+1)\Delta x]\xi^n - 2exp[j\beta_x p\Delta x]\xi^n \\ &\quad + exp[j\beta_x(p-1)\Delta x]\xi^n\} \\ &\quad - \frac{\varepsilon\mu}{(\Delta t)^2}\{exp[j\beta_x p\Delta x]\xi^{n+1} - 2exp[j\beta_x p\Delta x]\xi^n \\ &\quad + exp[j\beta_x p\Delta x]\xi^{n-1}\} = 0 \end{aligned} \tag{2.62}$$

Dividing Eq. (2.62) by $exp[j\beta_x p\Delta x]\xi^n$,

$$\frac{1}{(\Delta x)^2}\{exp[j\beta_x\Delta x] - 2 + exp[-j\beta_x\Delta x]\} - \frac{\varepsilon\mu}{(\Delta t)^2}\{\xi - 2 + \xi^{-1}\} = 0 \tag{2.63}$$

Dividing Eq. (2.63) by $\dfrac{\varepsilon\mu}{(\Delta t)^2\xi}$,

$$\frac{(\Delta t)^2\xi}{\varepsilon\mu}.\frac{1}{(\Delta x)^2}\{exp[j\beta_x\Delta x] - 2 + exp[-j\beta_x\Delta x]\} - \{\xi^2 - 2\xi + 1\} = 0 \tag{2.64}$$

Considering,

$$\begin{aligned} &\{exp[j\beta_x\Delta x] - 2 + exp[-j\beta_x\Delta x]\} \\ &\qquad = 2(\cos(\beta_x\Delta x) - 1) = -4\sin^2(\beta_x\frac{\Delta x}{2}) \end{aligned} \tag{2.65}$$

we get,

$$\{\xi^2 - 2\xi + 1\} + \left(\frac{4(\Delta t)^2}{\varepsilon\mu(\Delta x)^2}\sin^2\left(\beta_x\frac{\Delta x}{2}\right)\right)\xi = 0 \tag{2.66}$$

$$\xi^2 - 2\xi\left(1 - \frac{2(\Delta t)^2}{\varepsilon\mu(\Delta x)^2}\sin^2\left(\beta_x\frac{\Delta x}{2}\right)\right) + 1 = 0 \tag{2.67}$$

Let us defined a parameter A, as

$$A = 1 - \frac{2(\Delta t)^2}{\varepsilon\mu(\Delta x)^2}\sin^2\left(\beta_x\frac{\Delta x}{2}\right) \tag{2.68}$$

Thus, Eq. (2.67) becomes,

$$\xi^2 - 2\xi A + 1 = 0 \tag{2.69}$$

The roots of Eq. (2.69) are

$$\xi_1 = A + \sqrt{A^2 - 1} \tag{2.70}$$

$$\xi_2 = A - \sqrt{A^2 - 1} \tag{2.71}$$

According to Eq. (2.61) and since $\sin^2\theta \geq 0$, we get the relation

$$A = 1 - \frac{2(\Delta t)^2}{\varepsilon\mu(\Delta x)^2}\sin^2\left(\beta_x\frac{\Delta x}{2}\right) \leq 1 \tag{2.72}$$

Now, the stability condition can be specify in terms of A

Case (1): $A < -1$

According to Eq. (2.72), and since $1 < |\xi_2|$, the field is unstable.

Case (2): $-1 \leq A \leq 1$

Since ξ_1 and ξ_2 can be expressed as

$$\xi_1 = A + \sqrt{A^2 - 1} = A + j\sqrt{1 - A^2} \tag{2.73}$$

$$\xi_2 = A - \sqrt{A^2 - 1} = A - j\sqrt{1 - A^2} \tag{2.74}$$

then,

$$|\xi_1| = |\xi_2| = A^2 + 1 - A^2 = 0 \tag{2.75}$$

Thus, the field is stable when

$$-1 \leq A \leq 1 \tag{2.76}$$

Now, from Eq. (2.68)

$$-1 \leq -\frac{2(\Delta t)^2}{\varepsilon\mu(\Delta x)^2}\sin^2\left(\beta_x\frac{\Delta x}{2}\right) + 1 \leq 1 \tag{2.77}$$

from Eq. (2.72) the relation between the center terms and the right-hand term is always satisfied, so we have to consider only the left-hand term and center term

$$-1 \leq -\frac{2(\Delta t)^2}{\varepsilon\mu(\Delta x)^2}\sin^2\left(\beta_x\frac{\Delta x}{2}\right)+1 \tag{2.78}$$

Considering the case in which the right-hand side reaches its maximum, that is when $\sin^2(0)=1$

$$-1 \leq -\frac{2(\Delta t)^2}{\varepsilon\mu(\Delta x)^2}+1 \tag{2.79}$$

Subtract (-1) from each sides

$$-2 \leq -\frac{2(\Delta t)^2}{\varepsilon\mu(\Delta x)^2} \tag{2.80}$$

Thus, we get

$$1 \geq \frac{(\Delta t)^2}{\varepsilon\mu(\Delta x)^2} \tag{2.81}$$

and therefore

$$\varepsilon\mu\left(\frac{1}{(\Delta x)^2}\right)^{-1} \geq (\Delta t)^2 \tag{2.82}$$

Now, we can rewrite this relation as the restriction on the time step Δt

$$\Delta t \leq \sqrt{\varepsilon\mu}\left(\frac{1}{(\Delta x)^2}\right)^{-1/2} = \frac{\sqrt{\varepsilon_r\mu_r}}{c_0}\left(\frac{1}{(\Delta x)^2}\right)^{-1/2} = \frac{1}{v}\left(\frac{1}{(\Delta x)^2}\right)^{-1/2} \tag{2.83}$$

where, $\mu_r = 1$, Δx is the spatial discretization width and Δt is the time step and c_0, ε_r and $v = c_0/\sqrt{\varepsilon_r}$ are respectively the velocity of the light in the vacuum, the relative permittivity of the medium, and velocity of the light in the medium.

For a three dimension structure, the corresponding restriction is

$$\Delta t \leq \frac{1}{v}\left(\frac{1}{(\Delta x)^2}+\frac{1}{(\Delta y)^2}+\frac{1}{(\Delta z)^2}\right)^{-1/2} \tag{2.84}$$

According to Eq. (2.84), the time step Δt must be bounded in order to avoid numerical instability. Numerical instability is an undesirable possibility with explicit numerical differential equation solvers that can cause the computed results to spuriously increase without limit as time-marching continues.

2.4 Finite Difference Frequency Domain (FDFD)

The Finite Difference Frequency Domain (FDFD) is a numerical solution for problems in electromagnetics which operates in the frequency domain [41-45]. The

FDFD method is based on finite-difference approximations of the derivative operators in the differential equation being solved. Because the method uses the frequency domain equations, the results yield only a single-frequency, steady-state solution. FDFD maintains the spatial features of FDTD method, but removes time stepping.

2.4.1 FDFD from Maxwell's Equations

Using the differential form of Ampere's Law and Faraday's Law in frequency domain are given as

$$\text{Ampere's Law} \qquad j\omega\mu\boldsymbol{H} = -\boldsymbol{\nabla}\times\mathbf{E} \tag{2.85}$$

$$\text{Faraday's Law} \qquad j\omega\varepsilon\boldsymbol{E} = \boldsymbol{\nabla}\times\mathbf{H} \tag{2.86}$$

Consider a one dimension case, for x-directed propagation and **E** polarized along *y*-direction are

$$j\omega\mu H_z = -\frac{\partial \mathrm{E}_y}{\partial x} \tag{2.87}$$

$$j\omega\varepsilon E_y = -\frac{\partial \mathrm{H}_z}{\partial x} \tag{2.88}$$

Discretizing using the Leapfrog Method [46], we have the finite difference equations

$$j\omega\mu H_z\big|_{i+\frac{1}{2}} = -\frac{\mathrm{E}_y|_{i+1} - \mathrm{E}_y|_i}{\Delta x} \tag{2.89}$$

$$j\omega\varepsilon \mathrm{E}_y|_i = -\frac{H_z\big|_{i+\frac{1}{2}} - H_z\big|_{i-\frac{1}{2}}}{\Delta x} \tag{2.90}$$

Now, Eq. (2.89) and Eq. (2.90) can be written as a simple linear system as

$$A_h H_z\big|_{i+\frac{1}{2}} + \mathrm{E}_y|_{i+1} - \mathrm{E}_y|_i = 0 \tag{2.91}$$

$$A_e \mathrm{E}_y|_i + H_z\big|_{i+\frac{1}{2}} - H_z\big|_{i-\frac{1}{2}} = 0 \tag{2.92}$$

where, $A_h = j\omega\mu\Delta x$ and $A_e = j\omega\varepsilon\Delta x$.The FDFD method is useful when the source wave can be approximated by a single frequency.

CHAPTER 3

3. Plasmonic Thin Film Solar Cell

3.1 Introduction

In this chapter, a plasmonic thin-film solar cell with the periodic strip structure is studied. The optical design of the device structure is important for optimizing the performance for thin-film SCs.

Figure 3.1shows the schematic diagram of a solar structure model with the textured back reflector (BR) and the antireflection (AR) coatings. As a light-trapping configuration, the textured BRs are proposed for extending the optical path length [47-49]. However, the configuration might suffer from the back surface recombination loss. The textured AR coating is used to reduce the reflection of light at the top surface of the SCs [50]. However, the AR coating cannot employ the sufficient light concentration. So, a better light trapping and concentration schemes are needed for improving the efficiency of SCs.

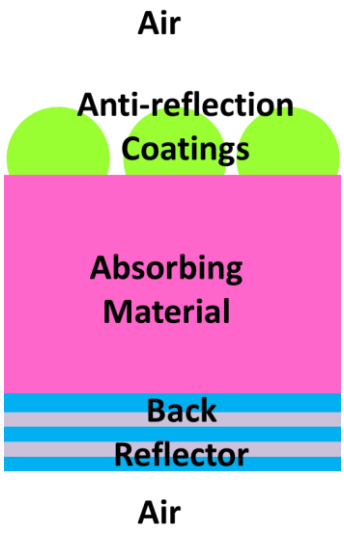

Figure 3.1: The schematic diagram of a solar cell structure[51].

Surface Plasmon Resonances (SPRs) are the collective oscillation of the free electrons that are restricted to surfaces and interact with light producing a polariton [52]. SPRs occur at the interface between a dielectric with the positive dielectric constant ε_r^d and a metal with the negative dielectric constantε_r^m. However, SPRs only exist when Re$(-\varepsilon_r^m > \varepsilon_r^d)$ is satisfied [53, 54]. Moreover, in order to excite the SPRs by light, it is required a coupling technique that providing a wavevector mismatch [55-60].

Maxwell's equations will be solved in order to describe the propagation and scattering of sunlight within the solar cell. The Finite Different Frequency Domain method (FDFD) is used to discretize the inhomogeneous wave function for modeling the plasmonic thin-film solar cell [61-63].

3.2 Theoretical Modeling

A two-dimensional plasmonic thin-film silicon structure with a p-polarized incident light with the electromagnetic component of H_z, E_x andE_y. The exp$(j\omega t)$ time convention is used. For the solar cells, all materials are non-magnetic (i.e. $\mu_r = 1$). SPRs are excited by the metallic periodic nanostructures and subwavelength scatterers. The unit cell of the plasmonic thin film solar cell is shown in Figure 3.2.

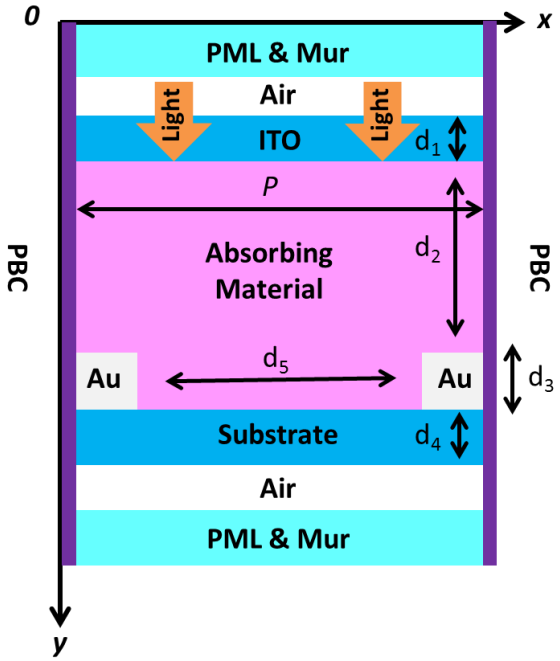

Figure 3.2: The unit cell of the plasmonic thin-film solar cell [51].

The structure contains four layers which include indium tin oxide (ITO), absorbing materials, Au electrodes, and substrate with thickness of d_1, d_2, d_3, and d_4, respectively. The distance between the two adjacent strips is d_5 and the periodicity is *P*. The PML and the Mur absorbing boundary conditions are imposed at the top and the bottom of the solar cell structure. The periodic boundary conditions (PBC) are employed at the left and right sides of the unit cell. Figure 3.3 shows the inhomogeneous material treatment. Where, the squares denote the five differences nodes. The center square is enclosed by the four rectangular regions with varies dielectric constants [51].

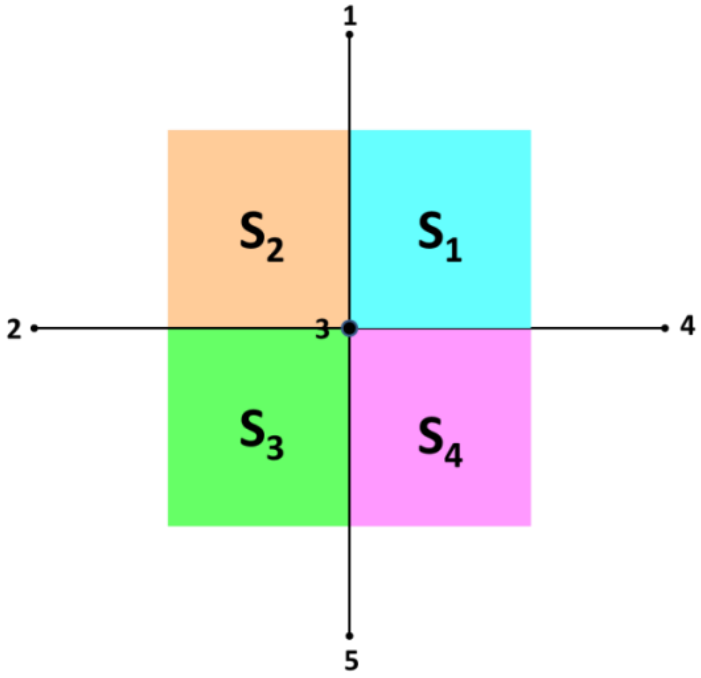

Figure 3.3: The inhomogeneous material treatment.

3.2.1 Finite Difference Equations

For the two dimension isotropic and inhomogeneous media, the wave equation of the total field H_z^t is given by [64]

$$\frac{\partial}{\partial x}\left(\frac{1}{\varepsilon_r(x,y)}\frac{\partial H_z^t}{\partial x}\right)+\frac{\partial}{\partial y}\left(\frac{1}{\varepsilon_r(x,y)}\frac{\partial H_z^t}{\partial y}\right)+k_0^2 H_z^t=0 \tag{3.1}$$

where, $\varepsilon_r(x,y)$ is the complex dielectric constant, k_0^2 is the wave number of free space. Using the Second-Order central differences, we get

$$\begin{aligned}&\frac{\partial}{\partial x}\left(\frac{1}{\varepsilon_r(x,y)}\frac{\partial H_z^t}{\partial x}\right)\\&=\frac{1}{\Delta_x}\left(\frac{H_z^t(i+1,j)-H_z^t(i,j)}{\varepsilon_r\left(i+\frac{1}{2},j\right)\Delta_x}\right.\\&\left.-\frac{H_z^t(i,j)-H_z^t(i-1,j)}{\varepsilon_r\left(i-\frac{1}{2},j\right)\Delta_x}\right)+\mathcal{O}(\Delta_x^2)\end{aligned} \tag{3.2}$$

where, $\Delta_x$is the spatial step in the x-direction. Now dielectric constants can be averaged as

$$\frac{1}{\varepsilon_r(i+\frac{1}{2},j)}\approx\frac{1}{2}\left(\frac{1}{\varepsilon_{r1}}+\frac{1}{\varepsilon_{r4}}\right) \tag{3.3}$$

$$\frac{1}{\varepsilon_r(i-\frac{1}{2},j)}\approx\frac{1}{2}\left(\frac{1}{\varepsilon_{r2}}+\frac{1}{\varepsilon_{r3}}\right) \tag{3.4}$$

where, the subscript 1, 2, 3, and 4 refer to the small rectangular regions as shown in Figure 3.3.

Using the notations of

$$\boldsymbol{\phi_1}=H_z^t(i,j-1) \tag{3.5}$$

$$\boldsymbol{\phi_2}=H_z^t(i-1,j) \tag{3.6}$$

$$\boldsymbol{\phi_3}=H_z^t(i,j) \tag{3.7}$$

$$\boldsymbol{\phi_4}=H_z^t(i+1,j) \tag{3.8}$$

$$\boldsymbol{\phi_5}=H_z^t(i,j+1) \tag{3.9}$$

The continuous inhomogeneous wave equation can be discretized into FDFD equations as

$$\sum_{m=1}^{5} c_m\boldsymbol{\phi}_m=0 \tag{3.10}$$

where,

$$c_1 = \frac{1}{2}\left(\frac{1}{\varepsilon_{r1}} + \frac{1}{\varepsilon_{r2}}\right).\frac{1}{\Delta_y^2} \tag{3.11}$$

$$c_2 = \frac{1}{2}\left(\frac{1}{\varepsilon_{r2}} + \frac{1}{\varepsilon_{r3}}\right).\frac{1}{\Delta_x^2} \tag{3.12}$$

$$c_3 = -\frac{1}{2}\left(\frac{1}{\varepsilon_{r1}} + \frac{1}{\varepsilon_{r2}} + \frac{1}{\varepsilon_{r3}} + \frac{1}{\varepsilon_{r4}}\right).\left(\frac{1}{\Delta_x^2} + \frac{1}{\Delta_y^2}\right) + k_0^2 \tag{3.13}$$

$$c_4 = \frac{1}{2}\left(\frac{1}{\varepsilon_{r4}} + \frac{1}{\varepsilon_{r1}}\right).\frac{1}{\Delta_x^2} \tag{3.14}$$

$$c_5 = \frac{1}{2}\left(\frac{1}{\varepsilon_{r3}} + \frac{1}{\varepsilon_{r4}}\right).\frac{1}{\Delta_y^2} \tag{3.15}$$

Now, the FDFD equation of scattered-field H_z^s can be derived by

$$H_z^t = H_z^{inc} + H_z^s \tag{3.16}$$

where, H_z^t is the total magnetic field, H_z^{inc} is the incident magnetic field and H_z^s is the scattered magnetic field.

3.2.2 Boundary Conditions

Boundary conditions are very crucial factors in the FDFD problems. If they are not defined, a non-unique solution is acquired. In case of a zero boundary conditions, the solution of the problem is zero.

As shown in Figure 3.2, the PML and Mur absorbing boundary condition are imposed at the top and the bottom of the solar cell structure. The Periodic Boundary Conditions (PBCs) are placed at the left and right sides of the unit cell.

The ABC's along the y-direction are used to limit the spurious reflections of the waves at the top and bottom boundaries of computational domain. The complex-coordinate PML [40, 65] is a virtuous ABC which has the form of

$$\frac{\partial^2 H_z^s}{\partial x^2} + \frac{1}{s_y}\frac{\partial}{\partial y}\left(\frac{1}{s_y}\frac{\partial H_z^s}{\partial y}\right) + k_0^2 H_z^s = 0 \tag{3.17}$$

where,

$$s_y = \begin{cases} 1 - j_0\dfrac{\sigma(y)}{\omega\varepsilon_0} & ,within\ PML \\ 1 & ,other \end{cases} \tag{3.18}$$

where, ε_0 is the permittivity of the free space, and ω is the angular frequency of the incident light.

The polynomial variation of the conductivities σ is employed, i.e.

$$\sigma(j) = \frac{C}{\Delta_y}\left(\frac{j-\frac{1}{2}}{L}\right)^{Q} \quad ,j = 1,2,3,\dots\dots\dots,8 \tag{3.19}$$

$$\sigma\left(j+\frac{1}{2}\right) = \frac{C}{\Delta_y}\left(\frac{j}{L}\right)^{Q} \quad ,j = 0,1,2,3,\dots\dots\dots,8 \tag{3.20}$$

where, L is the layer number of the PML, Q is the order of the polynomial, and C is a constant. For reducing the spurious numerical reflections, the optimized settings are set to $L = 8$, $Q = 3.7$, and $C = 0.02$. After submitting the previous values in Eqs. (3.19) and (3.20), we get

$$\sigma(j) = \frac{0.02}{\Delta_y}\left(\frac{j-\frac{1}{2}}{8}\right)^{3.7} \quad ,j = 1,2,3,\dots\dots\dots,8 \tag{3.21}$$

$$\sigma\left(j+\frac{1}{2}\right) = \frac{0.02}{\Delta_y}\left(\frac{j}{8}\right)^{3.7} \quad ,j = 0,1,2,3,\dots\dots\dots,8 \tag{3.22}$$

The convenient discretization form [41] for the coordinate-stretched term of Eq. (3.17) is given by

$$\begin{aligned}\frac{1}{s_y}\frac{\partial}{\partial y}\left(\frac{1}{s_y}\frac{\partial H_z^s}{\partial y}\right) &\\ \approx \frac{1}{s_y(j)\Delta_y}&\left[\frac{H_z^s(i,j+1)-H_z^s(i,j)}{s_y\left(j+\frac{1}{2}\right)\Delta_y}\right.\\ &\left.-\frac{H_z^s(i,j)-H_z^s(i,j-1)}{s_y\left(j-\frac{1}{2}\right)\Delta_y}\right]\end{aligned} \tag{3.23}$$

while the Perfectly Matched Layer (PML) do not work proficiently under periodic boundary condition [66], the hybrid absorbing boundary condition is proposed to reduce the spurious numerical reflections from the outmost boundary of the PML.

For example, at the top plane $y = 0$, the Second-Order Mur ABC can be written as

$$\left[\frac{\partial}{\partial y} - j_0\left(k_0 + \frac{1}{2k_0}\frac{\partial^2}{\partial x^2}\right)\right] H_z^s\Big|_{y=0} = 0 \tag{3.24}$$

Then, it can be discretized as

$$f_1 H_z^s(i,j) + f_2 H_z^s(i-1,j) + f_3 H_z^s(i+1,j) + f_4 H_z^s(i,j+1) = 0 \tag{3.25}$$

where,

$$f_1 = 2\exp\left(j_0 k_0 \Delta_y\right) - 2k_0^2\Delta_x^2 \exp\left(j_0 k_0 \Delta_y\right) - 2 \tag{3.26}$$

$$f_2 = f_3 = 1 - \exp\left(j_0 k_0 \Delta_y\right) \tag{3.27}$$

$$f_4 = 2k_0^2\Delta_x^2 \tag{3.28}$$

Due to the periodic geometry, the Floquet Theorem is used to implement the periodic boundary conditions along the x-direction,

$$H_z^s(x+P,y) = H_z^s(x,y)\exp(-j_0 k_0 cos\theta . P) \tag{3.29}$$

then,

$$H_z^s(x,y) = H_z^s(x+P,y)\exp(j_0 k_0 cos\theta . P) \tag{3.30}$$

where, P is the periodicity and θ is the incident angle with respect to x-direction. However, it can be noticed that Eq. (3.30) is hard to be treated using FDTD method compared to FDFD method, especially for the oblique incident case since the scattered-field value is unknown at a future time in periodic device structures.

For the horizontal interface ($y = y_h$) between media 1 and media 2, the one-sided difference scheme is used, and the boundary condition for the scattered magnetic field is

$$\frac{1}{\varepsilon_{r1}}\frac{\partial H_z^{s1}}{\partial y} - \frac{1}{\varepsilon_{r2}}\frac{\partial H_z^{s2}}{\partial y}\Big|_{y=y_h} = \frac{1}{\varepsilon_{r2}}\frac{\partial H_z^{inc}}{\partial y} - \frac{1}{\varepsilon_{r1}}\frac{\partial H_z^{inc}}{\partial y}\Big|_{y=y_h} \tag{3.31}$$

Using the High-Order-Accurate One-Sided Differences, we get

$$\frac{\partial H_z^{s1}}{\partial y}\Big|_{x=i\Delta_x} \approx \frac{1.5H_z^{s1}(i,j) - 2H_z^{s1}(i,j-1) + 0.5H_z^{s1}(i,j-2)}{\Delta_y} \tag{3.32}$$

$$\frac{\partial H_z^{s2}}{\partial y}\Big|_{x=i\Delta_x} \approx \frac{-1.5H_z^{s2}(i,j) + 2H_z^{s2}(i,j+1) - 0.5H_z^{s2}(i,j+2)}{\Delta_y} \tag{3.33}$$

3.2.3 Parameter Extraction

In this section, the parameters such as the Absorption Power Density η, the Zeroth-Order Reflectance R_p , and Transmittance T_p are extracted. The above FDFD equations and the boundary conditions to all free N nodes are applied in the solution region leading to the formation of a sparse matrix equation since only the nearest adjacent nodes affect the value of H_z^s at each node.

Then, the scattered magnetic field can be solved by the iterative methods with memory and computational complexity of $\mathcal{O}(N)$.

$$\frac{\partial H_z^s}{\partial x} = \frac{H_z^s(i+1,j) - H_z^s(i,j)}{\Delta_x} + \mathcal{O}(N) \tag{3.34}$$

$$\frac{\partial H_z^s}{\partial y} = \frac{H_z^s(i,j+1) - H_z^s(i,j)}{\Delta_y} + \mathcal{O}(N) \tag{3.35}$$

According to Eqs. (3.34) and (3.35), the FDFD equation of H_z^t is derived, and then the total electric field components are

$$E_x^t(i,j+\frac{1}{2}) \approx \frac{1}{2}\left(\frac{1}{\varepsilon_r(i,j+1)} + \frac{1}{\varepsilon_r(i,j)}\right).\left(\frac{H_z^t(i,j+1) - H_z^t(i,j)}{j_0\omega\varepsilon_0\Delta_y}\right) \tag{3.36}$$

$$E_y^t(i+\frac{1}{2},j) \approx \frac{1}{2}\left(\frac{1}{\varepsilon_r(i+1,j)} + \frac{1}{\varepsilon_r(i,j)}\right).\left(\frac{H_z^t(i+1,j) - H_z^t(i,j)}{-j_0\omega\varepsilon_0\Delta_x}\right) \tag{3.37}$$

The absorbing material per unit time per unit area, i.e.

$$\eta = \frac{\int_{S_a} \sigma_a |\mathrm{E}|^2 \, ds}{\Delta_{S_a}} \tag{3.38}$$

and since,

$$\sigma_a = -\omega\varepsilon_0 \mathrm{Im}(\varepsilon_{ra}) \tag{3.39}$$

then,

$$\eta = \frac{-\omega\varepsilon_0 \int_{S_a} \mathrm{Im}(\varepsilon_{ra}) |\mathrm{E}|^2 \, ds}{\Delta_{S_a}} \tag{3.40}$$

where, η is the power density, S_a is the region of the absorbing material, $\Delta_{S_a}$is the area of S_a and σ_a is the conductivity of the absorbing material.

The Zeroth-Order Reflectance R_p and Transmittance T_p are also vital parameters for optimizing the SC structures and they can be used to compare between the theoretical

and the experimental results. The Floquet's Theorem expresses the incident wave as a periodic function,

$$P(x) = \exp(-jkx).U(x) \tag{3.41}$$

$$P(x+d) = \exp(-jk(x+d)).U(x+d) \tag{3.42}$$

Since, $U(x)$ is a periodic function, then $U(x+d) = CU(x)$, where C is a complex constant.

$$P(x+d) = \exp\big(-jk(x+d)\big).CU(x) \tag{3.43}$$

Now, let $C = \exp(jkd)$,

$$P(x+d) = \exp\big(-jk(x+d)\big).\exp(jkd).U(x) \tag{3.44}$$

$$P(x+d) = \exp(-jkx).U(x) = P(x) \tag{3.45}$$

where, $P(x)$ is a periodic function with period of d. Using Fourier series, we get

$$P(x) = \sum_{n=-\infty}^{n=\infty} P_n \exp(j\frac{2\pi n}{d}x) \tag{3.46}$$

$$U(x) = \sum_{n=-\infty}^{n=\infty} P_n \exp(jk_{xn}x) \tag{3.47}$$

where, $k_x = k_0\cos(\phi^{inc})$.

Now, for the two-dimensional periodic structure with period of *P*, the Floquet modes are

$$\Psi_P = \exp(-jk_{xP}x)\exp(-jk_{yP}y) \tag{3.48}$$

where, $k_{xP} = k_0 cos\theta + \frac{2\pi n}{P}, P = 0, \pm1, \pm2, \ldots\ldots$

From the dispersion relation

$$k_0^2 = k_{xP}^2 + k_{yP}^2 \tag{3.49}$$

$$k_{yP} = \pm\sqrt{k_0^2 - k_{xP}^2} \tag{3.50}$$

then,

$$k_{yP} = \begin{cases} \sqrt{k_0^2 - k_{xP}^2}, & k_0^2 \geq k_{xP}^2 \\ -j\left|\sqrt{k_0^2 - k_{xP}^2}\right|, & k_0^2 < k_{xP}^2 \end{cases} \tag{3.51}$$

Based on the orthogonal properties of the Floquet modes, we get

$$R_P = \frac{\left|\frac{1}{P}\int_0^P H_z^s(x, y_r)\exp(jk_0 \cos\theta\, x)\, dx\right|^2}{A^2} \tag{3.52}$$

and

$$T_P = \frac{\left|\frac{1}{P}\int_0^P H_z^t(x, y_t)\exp(jk_0 \cos\theta\, x)\, dx\right|^2}{A^2} \tag{3.53}$$

where, P is the periodicity of the function, A is the amplitude of the incident light, y_r is the virtual boundaries for computing the Zeroth-Order Reflectance R_n, and y_t is the virtual boundaries for computing the Zeroth-Order Transmittance T_n.

3.2.4 Simulation Results

Consider a simple semi-infinite structure of A-Si/Au, the corresponding H_z field in the A-Si and Au layers can be written as

$$H_z(x, y) = \begin{cases} \exp\left(jk_y^{si}y - jk_x x\right), & k_y^{si} = \beta_y^{si} + j\alpha_y^{si}, \quad y < 0 \\ \exp\left(-jk_y^{Au}y - jk_x x\right), & k_y^{Au} = \beta_y^{Au} + j\alpha_y^{Au}, \quad y > 0 \end{cases} \tag{3.54}$$

where, k is the propagation constant, β is the phase constant, α is the attenuation constant.

For the p-polarized plane wave and with the assumption that ε_r^{Au} and ε_r^{si} are predominately real, the reflection coefficient of the up-going wave in the A-Si layer reflected by the Au layer is given by

$$R = \frac{\varepsilon_r^{Au}k_y^{si} - \varepsilon_r^{si}k_y^{Au}}{\varepsilon_r^{Au}k_y^{si} + \varepsilon_r^{si}k_y^{Au}} \tag{3.55}$$

where,

$$(k_y^{si})^2 = \varepsilon_r^{si}k_0^2 - k_x^2 \tag{3.56}$$

$$(k_y^{Au})^2 = \varepsilon_r^{Au}k_0^2 - k_x^2 \tag{3.57}$$

Now, the poles of Eq. (3.55) can be determined as,

$$\varepsilon_r^{Au}k_y^{si} + \varepsilon_r^{si}k_y^{Au} = 0 \tag{3.58}$$

$$k_x^2 = k_0^2\left(\frac{\varepsilon_r^{si}\varepsilon_r^{Au}}{\varepsilon_r^{si} + \varepsilon_r^{Au}}\right) \tag{3.59}$$

So, the x-directed propagation constant is

$$k_x = k_0 \left(\frac{\varepsilon_r^{si} \varepsilon_r^{Au}}{\varepsilon_r^{si} + \varepsilon_r^{Au}} \right)^{1/2}, k_x = \beta_x + i\alpha_x \tag{3.60}$$

In the previous case, we considered that both ε_r^{Au} and ε_r^{si} are predominately real. But for the real state, the loss of them must not be ignored. So that, the condition $\mathrm{Re}\left(-\varepsilon_r^{Au} > \varepsilon_r^{Si}\right)$ must be satisfied in order to excite the SPRs. Now, considering the complex dielectric constants and defending the attenuation and phase conditions for the formation of SPRs, the y-directed propagation constants in the A-Si and Au layers are the double-value functions of k_x .Taking into account that the SPRs is a surface wave decayed away from the dielectric-metal interface ($y = 0$), the attenuation constants conditions are

$$\alpha_y^{Si} < 0 \tag{3.61}$$

and

$$\alpha_y^{Au} < 0 \tag{3.62}$$

When the incident wavelength goes through the zero-crossing point of 560 nm, the eigenstates of Maxwell's Equations for the semi-infinite A-Si/Au structure become Surface Plasmon waves. As shown in Figure 3.4, the sign of the attenuation constant of the field at A-Si layer is changed as the incident wavelength goes through 560 nm.

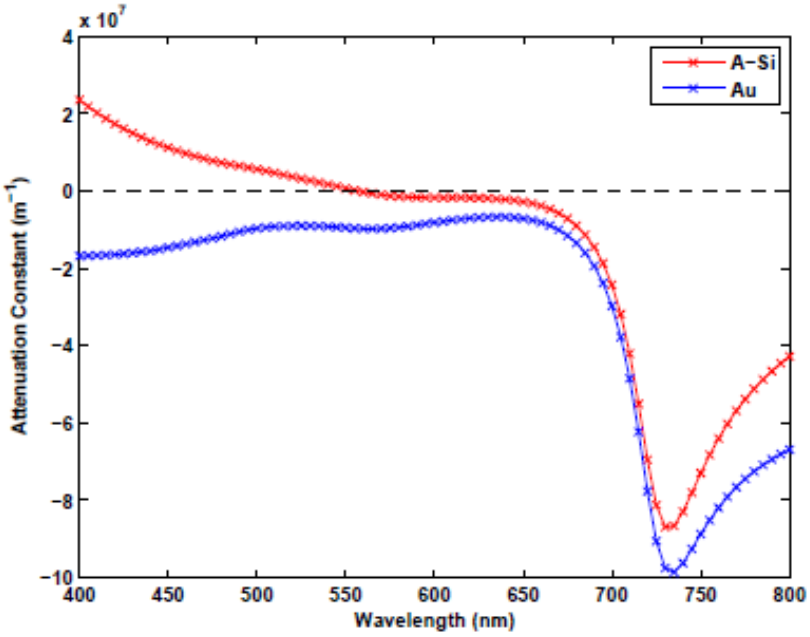

Figure 3.4: The y-directed attenuation constants in the A-Si and Au layers [51].

According to the Drude model, the metallic dielectric function can be approximated as

$$\varepsilon_r^{Au}(\omega) \approx 1 - \frac{\omega_P^2}{\omega^2} \tag{3.63}$$

where, ω_P : The plasma frequency of Au.

Thus, the SPRs exist at a long wavelength range where the metal is opaque. The SPRs exist when the incident wavelength is larger than 560nm. Moreover, the SPRs would be the eigenstates of the Maxwell's Equations for the semi-infinite A-Si/Au structure if the conditions in Eqs. (3.61) and (3.62) are satisfied. Also, the SPRs should satisfy the phase constants conditions, i.e.

$$\beta_y^{Si} < 0 \tag{3.64}$$

and

$$\beta_y^{Au} < 0 \tag{3.65}$$

The phase constants conditions accede to the oscillation property of the SPRs. Figure 3.5 shows the contour plot of the eigenstate for E_x field at 735nm, where the maximum phase constant β_x of the SPRs is executed by the resonance condition

$$\varepsilon_r^{Au} + \varepsilon_r^{si} \approx 0 \tag{3.66}$$

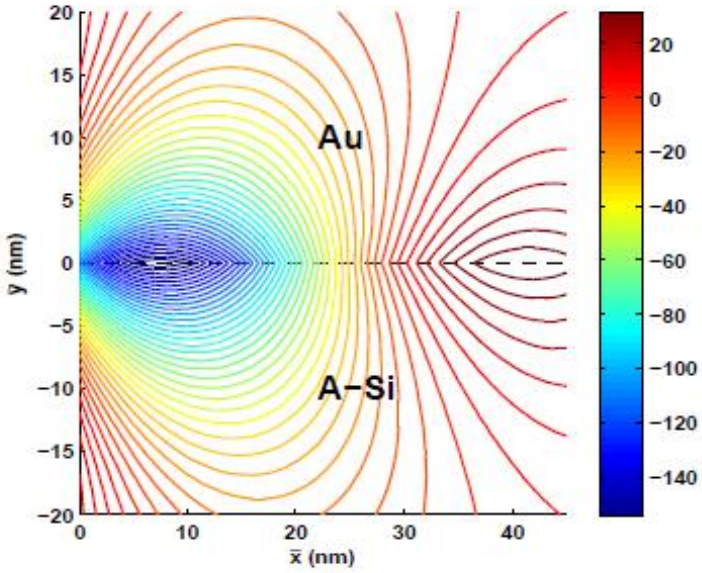

Figure 3.5: The contour plot of the eigenstate for E_x field at 735nm [51].

The field profile seems to be symmetric since k_x gets larger at 735nm and hence, k_y^{si} in Eq. (3.56) and k_y^{Au} in Eq. (3.57) are correspondent to each other.

For the periodic metal nanopatterns solar cell as shown in Figure 3.2, the absorbing material is A-Si and the substrate is glass (SiO_2). The complex dielectric constants of the material (Au, A-Si, etc.) are taken from [67, 68], where the geometric parameters of the device are set as d_1=25nm, d_2=120nm, d_3=40nm, d_4=30nm, d_5=100nm, and with a period of P=200nm. The y-directed incident field is the p-polarized plane wave with the amplitude of 1 and the frequency spectrum from 400nm to 800nm. The spatial step is set to$\Delta_x = \Delta_y = 0.5nm$. The Absorbed Power Density of the A-Si layer is shown in Figure 3.6.

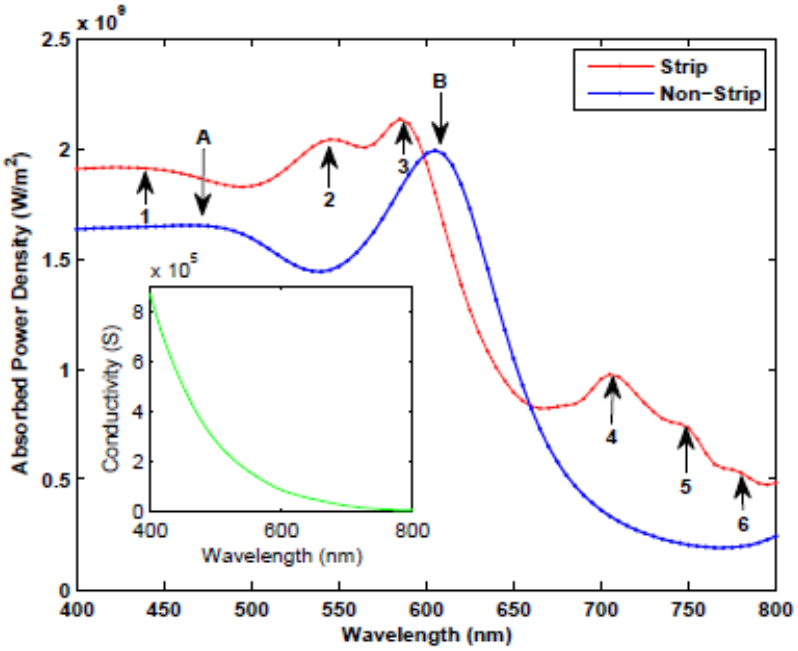

Figure 3.6: The Absorbed Power Density (η) by the A-Si for the periodic strip structure and the artificially periodic non-strip structure. The lower arrows from A to B refer to the absorption peaks of the non-strip structure and the upper arrows from 1 to 6 refer to the absorption peaks of the strip structure [51].

Now, using the planar Au layer, the non-strip structure can be modeled. Where, d_2 =140nm is adopted for attaining the same A-Si area and the other parameters are not changed. As shown in Figure 3.6, the A-Si bulk material has insufficient absorption from 650nm to 800nm because of its lower conductivity at the long wavelength region. The absorption η as expressed in Eq. (3.40) is significantly enhanced at the long wavelength region in both strip and non-strip structures. And this enhancement is related to the substantial increase of $|\mathrm{E}|^2$.

The strip structure displays stronger absorption due to the excited SPRs and the constructive interference between strips. Actuality, the external quantum efficiency can be enhanced by the efficient absorption.

Along the $\pm$y directions, consider a multilayered medium structure. The waveguide modes can approximately established by computing Generalized Reflection Coefficient $\tilde{R}_{i,i+1}$ of the medium between the ith layer and the (i+1)th layer,

$$\tilde{R}_{i,i+1} = \frac{R_{i,i+1} + \tilde{R}_{i+1,i+2} e^{-2jk_{i+1,y}(d_{i+1}-d_i)}}{1 + R_{i,i+1}\tilde{R}_{i+1,i+2} e^{-2jk_{i+1,y}(d_{i+1}-d_i)}} \quad (3.67)$$

where,$(d_{i+1} - d_i)$ is the thickness of the (i+1)th layer.

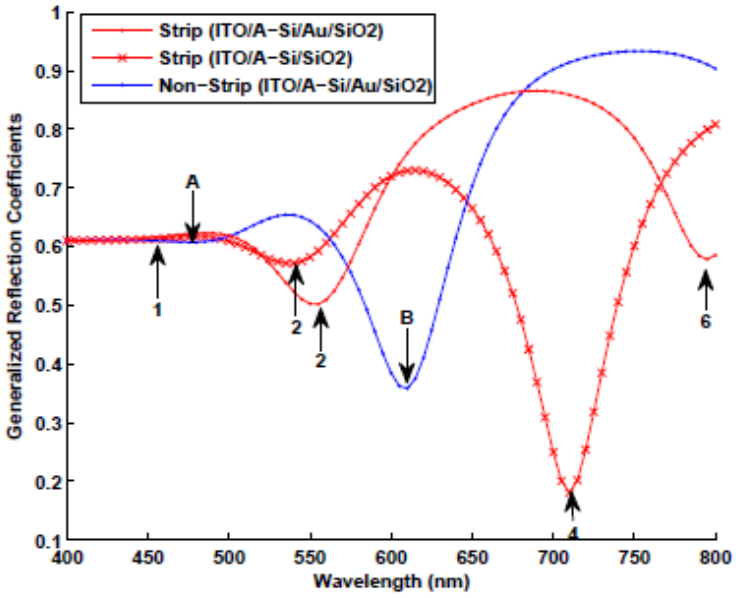

Figure 3.7 : The Generalized Reflection Coefficients for locating the waveguide modes. The dips of the Generalized Reflection Coefficients correspond to some absorption peaks of Figure 3.6 [51].

In case of a y-directed plane wave excitation, we have

$$k_{i+1,y} = k_{i+1} = k_0\sqrt{\varepsilon_{r,i+1}} \quad (3.68)$$

As shown in Figure 3.7, the waveguide modes can be obtained from the local minima of the Generalized Reflection Coefficient. From Figure 3.7, the waveguide modes contribute to all the absorption peaks (A and B) of the non-strip structure. The interface between the A-Si and Au layers can be treated as a good mirror for trapping the light in the non-strip structure and this explains the absorption enhancement that happens in the planar structure.

In the non-strip structure, the SPRs cannot be excited because of the momentum mismatch. However, in the strip structure, there are two different multilayered media as shown in Figure 3.2. In the Au strips region, the medium is Air/ITO/A-Si/Au/SiO_2/Air. In the other region, the medium is Air/ITO/A-Si/SiO_2/Air. As shown in Figure 3.6, the waveguide modes of the former medium are due to the absorption peaks 1, 2, and 6, where the absorption peaks 2 and 4 are contributed to the waveguide modes of the medium without the Au strip.

As shown in Figure 3.4 and Figure 3.6, the SPRs is successfully excited by the sub-scatterer strip at the wavelength 745nm. Based on the mode conversion theory, the sub-wavelength strip can excite the evanescent wave components and that provides the momentum mismatch Δk with the continuous spectrum up to $2\pi/d_3$. The x-directed boundaries of the strip achieve better field concentration than the y-directed boundaries.

3.3 Conclusion

The FDFD is used to develop an efficient model of a thin-film plasmonic solar cell with a periodic strip. The hybrid ABC shows better efficiency than the PML for the periodic structure. The material discontinuities are treated using the inhomogeneous wave equation and the one-sided difference scheme. The attenuation and phase constants conditions of the SPRs are discussed for lossy material systems.

For the semi-infinite dielectric-metal structure, the SPRs exist if the vertical phase and attenuation constants are negative in both dielectric and metal layers. The sub-wavelength scatterers can excite the evanescent waves, which provide the size-dependent continues spectrum components. Thus, the subwavelength scatterers can excite the SPRs for the broadband light enhancement.

Using the waveguide mode, the Floquet mode and the SPRs, the absorption peaks are explained for the periodic strip solar cell structure. Via changing the geometric parameters, the peaks locations can be modified for optimizing the performance of the solar cell.

CHAPTER 4

4. Simulation of Thin Film Solar Cell Waveguide Structure Using Finite Difference Time Domain

4.1 Introduction

For an efficient thin-film solar cell, we need to reduce the cost of its manufacturing, and increase the power conversion efficiency. A light-trapping scheme can help to achieve the previous purposes. Surface Plasmons are used as an efficient light-trapping technique. The optical absorption of thin-film solar cells can be improved by the extremely near-field enhancement inherent from the Surface Plasmons. In this section, the plasmonic effect in thin-film solar cell is studied. FDTD is used to simulate the same thin-film solar cell nanostructure as in chapter 2. An incident *p*-polarized plane wave is propagating vertically into the plasmonic solar cell. Auxiliary Differential Equation Technique (ADE) and Lorentz model are applied to simulate the dispersive materials including the absorbing material (amorphous silicon: A-Si) and metal (Au) [69].

4.2 Theoretical Modeling

The total electric field can be expressed as a sum of both the incident and scattered electric field as

$$\mathbf{E}_{total} = \mathbf{E}_{inc} + \mathbf{E}_{scatt} \tag{4.1}$$

The total magnetic field can also be expressed as a sum of both the incident and scattered magnetic field

$$\mathbf{H}_{total} = \mathbf{H}_{inc} + \mathbf{H}_{scatt} \tag{4.2}$$

For an incident field in free space, Ampere's Law is

$$\varepsilon_0 \frac{\partial \mathbf{E}_{inc}}{\partial t} = \nabla \times \mathbf{H}_{inc} \tag{4.3}$$

For dispersive medium, the total field can be expressed as

$$\nabla \times \mathbf{H}_{total} = \varepsilon_0 \varepsilon_\infty \frac{\partial \mathbf{E}_{total}}{\partial t} + \sum_{P=1}^{P} \mathbf{J}_{P,total} \tag{4.4}$$

where, P is the pole-pair of the Lorentz medium.

For Lorentz media, the polarization current density is

$$\omega_P^2 \mathbf{J}_{\mathrm{P,total}} + 2\delta_P \frac{\partial \mathbf{J}_{\mathrm{P,total}}}{\partial t} - \frac{\partial^2 \mathbf{J}_{\mathrm{P,total}}}{\partial t^2} = \varepsilon_0(\varepsilon_s - \varepsilon_\infty)\omega_P^2 \frac{\partial \mathbf{E}_{total}}{\partial t} \tag{4.5}$$

where, ε_s is the static permittivity.

Applying the finite difference to the partial differential terms

$$\begin{aligned} \omega_P^2 \mathbf{J}_{\mathrm{P,total}} + 2\delta_P \frac{\mathbf{J}_{P,total}^{n+1} - \mathbf{J}_{P,total}^{n-1}}{2\Delta t} - \frac{\mathbf{J}_{P,total}^{n+1} - 2\mathbf{J}_{P,total}^{n} + \mathbf{J}_{P,total}^{n-1}}{(\Delta t)^2} \\ = \varepsilon_0(\varepsilon_s - \varepsilon_\infty)\omega_P^2 \frac{\mathbf{E}_{total}^{n+1} - \mathbf{E}_{total}^{n-1}}{2\Delta t} \end{aligned} \tag{4.6}$$

Hence, the update equation for the phasor polarization current is

$$\mathbf{J}_{P,total}^{n+1} = \alpha_P \mathbf{J}_{P,total}^{n} + \xi_P \mathbf{J}_{P,total}^{n-1} + \gamma_P \frac{\mathbf{E}_{total}^{n+1} - \mathbf{E}_{total}^{n-1}}{2\Delta t} \tag{4.7}$$

where,

$$\alpha_P = \frac{2 - \omega_P^2 (\Delta t)^2}{\xi_P \Delta t + 1} \tag{4.8}$$

$$\xi_P = \frac{\delta_P \Delta t - 1}{\delta_P \Delta t + 1} \tag{4.9}$$

and

$$\gamma_P = \frac{\varepsilon_0(\varepsilon_s - \varepsilon_\infty)\omega_P^2 (\Delta t)^2}{\delta_P \Delta t + 1} \tag{4.10}$$

By applying a time-averaging for the two terms at (n) and $(n+1)$, the polarization current $\mathbf{J}_{total}$ can be presented at time $(n + \frac{1}{2})$

$$\mathbf{J}_{P,total}^{n+\frac{1}{2}} = \frac{1}{2}\left(\mathbf{J}_{P,total}^{n+1} + \mathbf{J}_{P,total}^{n}\right)$$
$$= \frac{1}{2}\Bigg((1+\alpha_P)\mathbf{J}_{P,total}^{n} + \xi_P \mathbf{J}_{P,total}^{n-1} + \frac{\gamma_P}{2\Delta t}\left(\mathbf{E}_{total}^{n+1} - \mathbf{E}_{total}^{n-1}\right)\Bigg) \tag{4.11}$$

Then, the electric field $\mathbf{E}$ can be updated from time step (n) to time step $(n+1)$ using the following equation

$$\mathbf{E}_{total}^{n+1} = \frac{\sum_{P=1}^{P}\gamma_P}{4\varepsilon_0\varepsilon_\infty + \sum_{P=1}^{P}\gamma_P}\mathbf{E}_{total}^{n-1} + \frac{2\varepsilon_0\varepsilon_\infty}{2\varepsilon_0\varepsilon_\infty + \frac{1}{2}\sum_{P=1}^{P}\gamma_P}\mathbf{E}_{total}^{n}$$
$$+ \frac{2\Delta t}{2\varepsilon_0\varepsilon_\infty + \frac{1}{2}\sum_{P=1}^{P}\gamma_P}\Bigg\{\nabla \times \mathbf{H}^{n+\frac{1}{2}} - \frac{1}{2}\sum_{P=1}^{P}(1+\alpha_P)\mathbf{J}_{P,total}^{n} + \xi_P \mathbf{J}_{P,total}^{n-1}\Bigg\} \tag{4.12}$$

Now, using Eq. (4.1), Eq. (4.11) can be rewritten as,

$$\mathbf{E}_{inc}^{n+1} + \mathbf{E}_{scat}^{n+1} = \frac{\sum_{P=1}^{P}\gamma_P}{4\varepsilon_0\varepsilon_\infty + \sum_{P=1}^{P}\gamma_P}\left(\mathbf{E}_{inc}^{n-1} + \mathbf{E}_{scat}^{n-1}\right)$$
$$+ \frac{2\varepsilon_0\varepsilon_\infty}{2\varepsilon_0\varepsilon_\infty + \frac{1}{2}\sum_{P=1}^{P}\gamma_P t}\left(\mathbf{E}_{inc}^{n} + \mathbf{E}_{scat}^{n}\right)$$
$$+ \frac{2\Delta t}{2\varepsilon_0\varepsilon_\infty + \frac{1}{2}\sum_{P=1}^{P}\gamma_P}\Bigg\{\nabla \times \mathbf{H}_{inc}^{n+\frac{1}{2}} + \nabla \times \mathbf{H}_{scat}^{n+\frac{1}{2}} - \frac{1}{2}\sum_{P=1}^{P}(1+\alpha_P)\mathbf{J}_{P,total}^{n} + \xi_P \mathbf{J}_{P,total}^{n-1}\Bigg\} \tag{4.13}$$

Submitting Eq. (4. 2) in Eq. (4.12) and assuming a dispersive medium of a single Lorentz pole-pair $(P = 1)$, the resulting scattered electric field and total current density for the Lorentz model is:

$$\mathbf{E}_{scat}^{n+1} = \frac{1}{\varepsilon_0\varepsilon_\infty + \frac{\gamma}{4}} \cdot \left\{ (\varepsilon_0\varepsilon_\infty \mathbf{E}_{scat}^{n} + \frac{\gamma}{4}\mathbf{E}_{scat}^{n-1}) - \left(\varepsilon_0(\varepsilon_\infty - 1) + \frac{\gamma}{4}\right)\mathbf{E}_{inc}^{n+1} + \varepsilon_0(\varepsilon_\infty - 1)\mathbf{E}_{inc}^{n} + \frac{\gamma}{4}\mathbf{E}_{inc}^{n-1} - \frac{\Delta t}{2}\left[(1+\alpha)\cdot \mathbf{J}_{total}^{n} + \xi_P \mathbf{J}_{total}^{n-1} - 2\cdot(\nabla \times \mathbf{H}_{scat}^{n+\frac{1}{2}})\right]\right\} \quad (4.14)$$

where , $\alpha = \frac{2-\omega^2(\Delta t)^2}{\xi\Delta t+1}$, $\xi = \frac{\delta\Delta t-1}{\delta\Delta t+1}$ and $\gamma = \frac{\varepsilon_0(\varepsilon_s-\varepsilon_\infty)\omega^2(\Delta t)^2}{\delta\Delta t+1}$.

For solar cell, the electron-hole pair generation depends on the photon energy absorbed by the absorbing material per unit time per unit area, i.e.

$$\eta = \frac{\int_s \sigma(\omega)\left|\tilde{\mathbf{E}}(\omega,\mathbf{r})\right|^2 ds}{\Delta_s} = \frac{-\omega\varepsilon_0 \int_s [\mathrm{Im}\varepsilon_r(\omega)]\left|\tilde{\mathbf{E}}(\omega,\mathbf{r})\right|^2 ds}{\Delta_s} \quad (4.15)$$

where, η is the power density, *S* represents the region of the absorbing material, Δ_s is the area of *S*, and $\sigma(\omega) = -\omega\varepsilon_0 \mathrm{Im}[\varepsilon_r(\omega)]$ is the conductivity of the absorbing material.

4.2.1 Dispersion Relation

Consider a x-y plane as an interface plane, when a wave propagates in the x-direction, we get

$$\mathbf{E_1} = (E_{x1}, 0, E_{z1})\exp\big(j(k_x x - \omega t)\big)\exp(jk_{z1}z) \quad (4.16)$$

$$\mathbf{H_1} = (0, H_{y1}, 0)\exp\big(j(k_x x - \omega t)\big)\exp(jk_{z1}z) \quad (4.17)$$

$$\mathbf{E_2} = (E_{x2}, 0, E_{z2})\exp\big(j(k_x x - \omega t)\big)\exp(jk_{z2}z) \quad (4.18)$$

$$\mathbf{H_2} = (0, H_{y2}, 0)\exp\big(j(k_x x - \omega t)\big)\exp(jk_{z2}z) \quad (4.19)$$

Using Maxwell's Equations,

$$jk_x E_{x1} + jk_{z1}E_{z1} = 0, \qquad E_{z1} = -\frac{k_x}{k_{z1}}E_{x1} \quad (4.20)$$

$$jk_x E_{x2} + jk_{z1}E_{z2} = 0, \qquad E_{z2} = -\frac{k_x}{k_{z2}}E_{x2} \quad (4.21)$$

$$H_{y1} = \frac{\omega \varepsilon_0 \varepsilon_1}{k_{z1}} E_{x1} \tag{4.22}$$

$$H_{y2} = \frac{\omega \varepsilon_0 \varepsilon_2}{k_{z2}} E_{x2} \tag{4.23}$$

By applying the boundary conditions at $z = 0$,

$$H_{y1} = H_{y2}\,, \;\; E_{x1} = E_{x2} \tag{4.24}$$

thus,

$$\frac{\varepsilon_1}{k_{z1}} = \frac{\varepsilon_2}{k_{z2}} \tag{4.25}$$

also,

$$k_{z1} = -j(k_x^2 - \varepsilon_1 k^2)^{\frac{1}{2}}, \qquad k_x^2 > \varepsilon_1 k^2 \tag{4.26}$$

$$k_{z2} = -j(k_x^2 - \varepsilon_2 k^2)^{\frac{1}{2}}, \qquad k_x^2 > \varepsilon_2 k^2 \tag{4.27}$$

then,

$$k_x = k(\frac{\varepsilon_1 \varepsilon_2}{\varepsilon_1 + \varepsilon_2})^{\frac{1}{2}} \tag{4.28}$$

4.2.2 Simulation Results

For the two dimension thin film solar cell with periodic structure as shown in Figure 4.1, the absorbing material is A-Si, the electrode is Au and the substrate is SiO_2, the geometric parameters of the non-strip structure are set as d_1=25nm, d_2=140nm, d_3=40nm, d_4=30nm, d_5=100nm, and with a period of P=200nm, where the strip structure has the same geometric parameters except that d_2=140nm. The y-directed incident field is the p-polarized plane wave with the amplitude of 1 and the frequency spectrum is from 400nm to 800nm. The spatial step is set to $\Delta_x = \Delta_y = 0.5$nm.

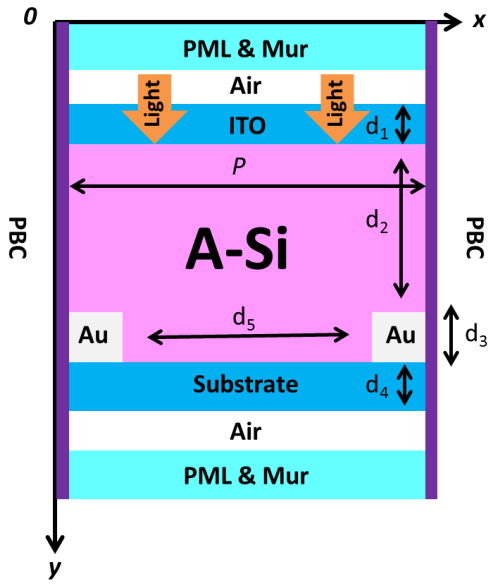

Figure 4.1: The unit cell of the plasmonic thin-film solar cell [51].

In the interface between a metal and dielectric, and based on the relation in Eq. (4.27), the momentum of surface plasmons [52, 71] is

$$k_{sp} = k\left(\frac{\varepsilon_m \varepsilon_a}{\varepsilon_m + \varepsilon_a}\right)^{\frac{1}{2}} \qquad (4.29)$$

where, ε_m and ε_a are the permittivities of metal and absorbing material, respectively. In order to excite the Surface Plasmons, the condition

$$\mathrm{Re}(-\varepsilon_m) > \mathrm{Re}(\varepsilon_a) \qquad (4.30)$$

should be satisfied. The momentum of Surface Plasmons, k_{sp} , is larger than the free space momentum, k_0 ,of the plane wave which ,in our study, is the sunlight. So that, an additional momentum must be provided in order to excite the Surface Plasmons.

The Generalized Reflection Coefficients of the strip and non-strip solar cell structures calculated by the FDTD method is shown in Figure 4.2. The case of strip structure shows much stronger absorption due to the excited Surface

Plasmons. However, in the non-strip structure, the Surface Plasmons cannot be excited due to the momentum mismatch.

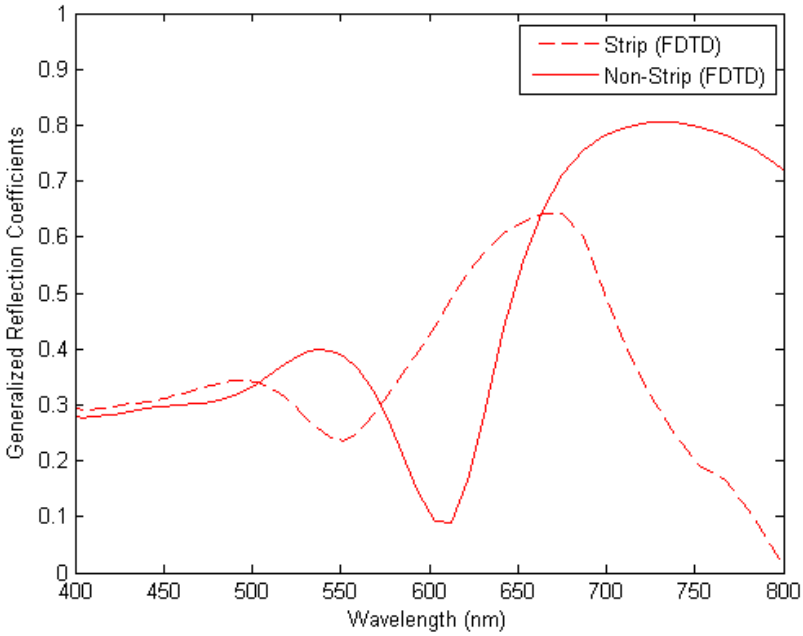

Figure 4.2: The Generalized Reflection Coefficients of the strip and non-strip solar cell structures calculated by the FDTD method [70].

The Absorbed Power Density of the A-Si layer is presented in Figure 4.3. It shows that Surface Plasmons excitation increases the absorption for the strip structure, where the Surface Plasmons cannot be excited in the non-strip structure due to the momentum mismatch. Also, it confirms the strong optical absorption of A-Si from 660-800nm which is similar to the results in Figure 4.2.

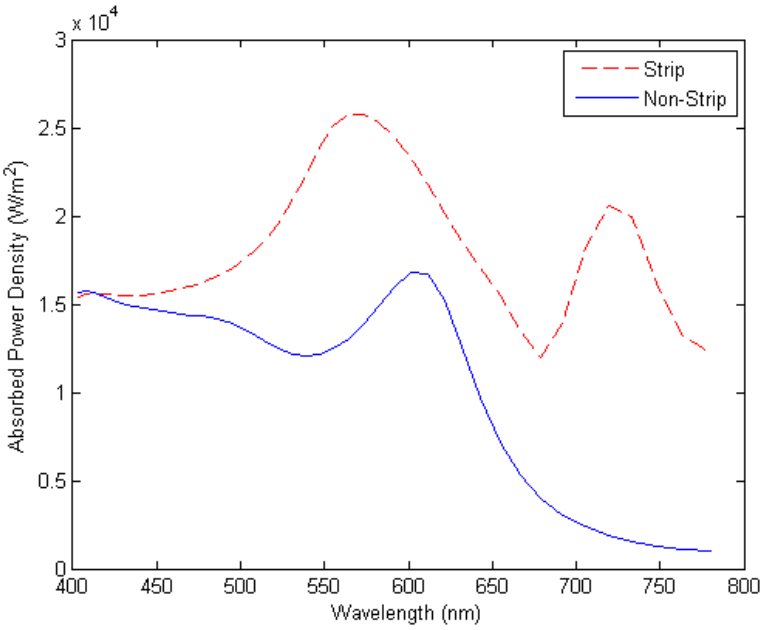

Figure 4.3: The Absorbed Power Density of the A-Si layer in the strip and non-strip solar cell structures [70].

4.3 Conclusions

The FDTD method is one of the simplest and strongest methods of the computational electromagnetic field. Due to the feature of flexibility and its easy implementation, FDTD method is a powerful tool in modeling inhomogeneous, anisotropic and dispersive media with periodic structure.

CHAPTER 5

5. Theoretical Approach of Metamaterials Waveguide Structure

5.1 Introduction

The Auxiliary Differential Equation method (ADE) is applied to simulate dispersive material [34, 72, 73] as Metamaterials. In ADE, the relation between **E** and **D** is expressed with a differential equation using the inverse Fourier Transformation of the relationship between **E**(ω) and **D**(ω) into the time domain.

In dispersive material, both the permittivity and permeability depend on frequency [74, 75]. The permittivity can be written as

$$\varepsilon_r(\omega) = \varepsilon_\infty + \sum_{P=1}^{P} \chi_P(\omega) \tag{5.1}$$

where $\varepsilon_r(\omega)$ is the relative permittivity, ε_∞ is the relative permittivity at infinite frequency, P is the number of poles and $\chi_P(\omega)$ is the susceptibility which denote the dispersive part of the relative permittivity.

Now, substituting Eq. (5.1) into Ampere's Law

$$\nabla \times \mathbf{H} = \sigma \mathbf{E} + \frac{\partial(\varepsilon \mathbf{E})}{\partial t} = \sigma \mathbf{E} + \varepsilon_0 \varepsilon_\infty \frac{\partial(\mathbf{E})}{\partial t} + \sum_{P=1}^{P} \mathbf{J}_P \tag{5.2}$$

$$\mathbf{J}_P = j\omega \varepsilon_0 \chi_P \mathbf{E} \tag{5.3}$$

where, Eq. (5.2) represents the Ampere's Law in time domain. $\mathbf{J}_P$ is the polarization current density. The term $\mathbf{J}_P$ has different forms for different dispersive material and it must be considered in the update of the FDTD field.

5.2 The Auxiliary Differential Equation for Debye Material

The single pole model for Debye material can be expressed as

$$\chi_P(\omega) = \frac{\varepsilon_{S,P} - \varepsilon_{\infty,P}}{1 + j\omega\tau_P} = \frac{\Delta\varepsilon_P}{1 + j\omega\tau_P} \tag{5.4}$$

where $\varepsilon_{S,P}$ is the static or zero-frequency relative permittivity, $\Delta\varepsilon_P = \varepsilon_{S,P} - \varepsilon_{\infty,P}$ is the change in relative permittivity due to the Debye pole, and τ_P is the pole relaxation time [76]. In case of Debye media with multiple poles, the permittivity function is

$$\varepsilon_r(\omega) = \varepsilon_{\infty,P} + \sum_{P=1}^{P} \frac{\Delta\varepsilon_P}{1 + j\omega\tau_P} \tag{5.5}$$

$$\check{\mathbf{J}}_P = \varepsilon_0 \Delta\varepsilon_P \left(\frac{j\omega}{1 + j\omega\tau_P}\right) \check{\mathbf{E}} \tag{5.6}$$

where $\check{\mathbf{J}}_P$is the phasor polarization current density associated with each pole. In FDTD, the phasor polarization current density $\check{\mathbf{J}}_P$ must be calculated in time domain. Thus, we first multiply both sides of Eq. (5.6) by $1 + j\omega\tau_P$

$$(1 + j\omega\tau_P)\check{\mathbf{J}}_P = \varepsilon_0 \Delta\varepsilon_P j\omega \check{\mathbf{E}} \tag{5.7}$$

Then, using the inverse Fourier Transformation Eq. (5.7) can be transformed as:

$$\mathbf{J}_\mathrm{P} + \tau_P \frac{\partial \mathbf{J}_\mathrm{P}}{\partial t} = \varepsilon_0 \Delta\varepsilon_P \frac{\partial \mathbf{E}}{\partial t} \tag{5.8}$$

Now, both of Eq. (5.2) and Eq. (5.8) represent the ADEs for the $\mathbf{J}_\mathrm{P}$ that is used to update the electric field equation. A semi-implicit finite-difference scheme centered at $(n + \frac{1}{2})$ is used for Eq. (5.8)

$$\mathbf{J}_P^{n+1} = k_P \mathbf{J}_P^n + \beta_P \left(\frac{\mathbf{E}^{n+1} - \mathbf{E}^n}{\Delta t}\right) \tag{5.9}$$

where,

$$k_P = \frac{1 - \frac{\Delta t}{2\tau_P}}{1 + \frac{\Delta t}{2\tau_P}} \tag{5.10}$$

and

$$\beta_P = \frac{\varepsilon_0 \Delta \varepsilon_P \frac{\Delta t}{\tau_P}}{1 + \frac{\Delta t}{2\tau_P}} \tag{5.11}$$

Since the electric field is updated using Eq. (5.2) with centered at time$(n + \frac{1}{2})$, the polarization current density **J** must be presenting at the same time step. In order to achieve that, an averaging of Eq. (5.9) at time (n) and $(n + 1)$ is applied,

$$\mathbf{J}_P^{n+\frac{1}{2}} = \frac{1}{2}(\mathbf{J}_P^n + \mathbf{J}_P^{n+1}) = \frac{1}{2}\left[(1 + k_P)\mathbf{J}_P^n + \beta_P\left(\frac{\mathbf{E}^{n+1} - \mathbf{E}^n}{\Delta t}\right)\right] \tag{5.12}$$

Now, Eq. (5.2) can be written as

$$\begin{aligned}\boldsymbol{\nabla} \times \mathbf{H}^{n+\frac{1}{2}} = \sigma\left(\frac{\mathbf{E}^{n+1} + \mathbf{E}^n}{2}\right) + \varepsilon_0\varepsilon_\infty\left(\frac{\mathbf{E}^{n+1} - \mathbf{E}^n}{\Delta t}\right) \\ + \frac{1}{2}\sum_{P=1}^{P}\left[(1 + k_P)\mathbf{J}_P^n + \beta_P\left(\frac{\mathbf{E}^{n+1} - \mathbf{E}^n}{\Delta t}\right)\right]\end{aligned} \tag{5.13}$$

The electric field **E** can be updated from time step (n) to time step $(n + 1)$ using the following equation

$$\begin{aligned}\mathbf{E}^{n+1} = \left(\frac{2\varepsilon_0\varepsilon_\infty + \sum_{P=1}^{P}\beta_P - \sigma\Delta t}{2\varepsilon_0\varepsilon_\infty + \sum_{P=1}^{P}\beta_P + \sigma\Delta t}\right)\mathbf{E}^n \\ + \left(\frac{2\Delta t}{2\varepsilon_0\varepsilon_\infty + \sum_{P=1}^{P}\beta_P + \sigma\Delta t}\right)\left[\boldsymbol{\nabla} \times \mathbf{H}^{n+\frac{1}{2}}\right. \\ \left. - \frac{1}{2}\sum_{P=1}^{P}(1 + k_P)\mathbf{J}_P^n\right]\end{aligned} \tag{5.14}$$

5.3 The Auxiliary Differential Equation for Lorentz Material

A Lorentz material with *P* pole pairs can be described with a relative permittivity function

$$\varepsilon_r(\omega) = \varepsilon_{\infty,P} + \sum_{P=1}^{P} \frac{\Delta\varepsilon_P \omega_P^2}{\omega_P^2 + 2j\omega\delta_P - \omega^2} \tag{5.15}$$

where $\varepsilon_r(\omega)$ is the relative permittivity, $\varepsilon_{\infty,P}$ is the relative permittivity at infinite frequency, P is the number of poles, $\Delta\varepsilon_P = \varepsilon_{S,P} - \varepsilon_{\infty,P}$ is the change in relative permittivity due to the Lorentz pole pair, ω_P is the frequency of the pole pair and δ_P is the damping coefficient [77]. The phasor polarization current is associated with the pole pair of the susceptibility function

$$\check{\mathbf{J}}_P = j\omega \left(\frac{\varepsilon_0 \Delta\varepsilon_P \omega_P^2}{\omega_P^2 + 2j\omega\delta_P - \omega^2} \right) \check{\mathbf{E}} \tag{5.16}$$

In FDTD, the phasor polarization current density $\check{\mathbf{J}}_P$ must be calculated in time domain. Thus, we first multiply both sides of Eq. (5.16) by$\omega_P^2 + 2j\omega\delta_P - \omega^2$,

$$(\omega_P^2 + 2j\omega\delta_P - \omega^2)\check{\mathbf{J}}_P = j\omega\varepsilon_0 \Delta\varepsilon_P \omega_P^2 \check{\mathbf{E}} \tag{5.17}$$

then, using the inverse Fourier Transformation Eq. (5.17) can be transformed as:

$$\omega_P^2 \mathbf{J}_P + 2\delta_P \frac{\partial \mathbf{J}_\mathrm{P}}{\partial t} - \frac{\partial^2 \mathbf{J}_\mathrm{P}}{\partial t^2} = \varepsilon_0 \Delta\varepsilon_P \omega_P^2 \frac{\partial \mathbf{E}}{\partial t} \tag{5.18}$$

Now, both of Eq. (5.2) and Eq. (5.18) represent the ADEs for the $\mathbf{J}_\mathrm{P}$ that is used to update the electric field equation.

Now, applying the finite difference to the partial differential terms

$$\begin{aligned} \omega_P^2 \mathbf{J}_P^n + 2\delta_P \frac{\mathbf{J}_P^{n+1} - \mathbf{J}_P^{n-1}}{2\Delta t} - \frac{\mathbf{J}_P^{n+1} - 2\mathbf{J}_P^n + \mathbf{J}_P^{n-1}}{(\Delta t)^2} \\ = \varepsilon_0 \Delta\varepsilon_P \omega_P^2 \frac{\mathbf{E}^{n+1} - \mathbf{E}^{n-1}}{2\Delta t} \end{aligned} \tag{5.19}$$

Thus, the update equation for the phasor polarization current density is

$$\mathbf{J}_P^{n+1} = \alpha_P \mathbf{J}_P^n + \xi_P \mathbf{J}_P^{n-1} + \gamma_P \frac{\mathbf{E}^{n+1} - \mathbf{E}^{n-1}}{2\Delta t} \tag{5.20}$$

where,

$$\alpha_P = \frac{2 - \omega_P^2 (\Delta t)^2}{\delta_P \Delta t + 1} \tag{5.21}$$

$$\xi_P = \frac{\delta_P \Delta t - 1}{\delta_P \Delta t + 1} \tag{5.22}$$

and

$$\gamma_P = \frac{\varepsilon_0 \Delta \varepsilon_P \omega_P^2 (\Delta t)^2}{\delta_P \Delta t + 1} \tag{5.23}$$

By time-averaging for the two terms at (n) and $(n+1)$, the polarization current density $\mathbf{J}$ can presented at time $(n+\frac{1}{2})$, we get

$$\begin{aligned} \mathbf{J}_P^{n+\frac{1}{2}} &= \frac{1}{2}(\mathbf{J}_P^{n+1} + \mathbf{J}_P^n) \\ &= \frac{1}{2}\left((1+\alpha_P)\mathbf{J}_P^n + \xi_P \mathbf{J}_P^{n-1} + \frac{\gamma_P}{2\Delta t}(\mathbf{E}^{n+1} - \mathbf{E}^{n-1})\right) \end{aligned} \tag{5.24}$$

Thus, Ampere's Law takes the form of

$$\begin{aligned} \nabla \times \mathbf{H}^{n+\frac{1}{2}} = \sigma\left(\frac{\mathbf{E}^{n+1} + \mathbf{E}^n}{2}\right) + \varepsilon_0 \varepsilon_\infty \left(\frac{\mathbf{E}^{n+1} - \mathbf{E}^n}{\Delta t}\right) \\ + \frac{1}{2}\sum_{P=1}^{P}\left[(1+\alpha_P)\mathbf{J}_P^n + \xi_P \mathbf{J}_P^{n-1} + \frac{\gamma_P}{2\Delta t}(\mathbf{E}^{n+1} - \mathbf{E}^{n-1})\right] \end{aligned} \tag{5.25}$$

Then, the electric field $\mathbf{E}$ can be updated from time step (n) to time step $(n+1)$ using the following equation

$$\begin{aligned} \mathbf{E}^{n+1} = \frac{\sum_{P=1}^{P}\gamma_P}{4\varepsilon_0\varepsilon_\infty + \sum_{P=1}^{P}\gamma_P + \sigma\Delta t}\mathbf{E}^{n-1} + \frac{2\varepsilon_0\varepsilon_\infty - \sigma\Delta t}{2\varepsilon_0\varepsilon_\infty + \frac{1}{2}\sum_{P=1}^{P}\gamma_P + \sigma\Delta t}\mathbf{E}^n \\ + \frac{2\Delta t}{2\varepsilon_0\varepsilon_\infty + \frac{1}{2}\sum_{P=1}^{P}\gamma_P + \sigma\Delta t}\left\{\nabla \times \mathbf{H}^{n+\frac{1}{2}}\right. \\ \left. - \frac{1}{2}\sum_{P=1}^{P}(1+\alpha_P)\mathbf{J}_P^n + \xi_P \mathbf{J}_P^{n-1}\right\} \end{aligned} \tag{5.26}$$

5.4 The Auxiliary Differential Equation of Drude Material

Consider a multi-pole Drude material with a permittivity function as [78]

$$\varepsilon_r(\omega) = \varepsilon_{\infty,P} - \sum_{P=1}^{P} \frac{\omega_P^2}{\omega^2 - j\omega\gamma_P} \tag{5.27}$$

where, P is the number of poles, $\varepsilon_{\infty,P}$ is the relative permittivity at infinite frequency, ω_P is the frequency of the P^{th}pole and γ_P is the inverse of the P^{th}pole relaxation time [79]. The frequency domain polarization current for P^{th}pole is

$$\check{\mathbf{J}}_P = -j\omega\varepsilon_0 \left(\frac{\omega_P^2}{\omega^2 - j\omega\gamma_P} \right) \check{\mathbf{E}} \tag{5.28}$$

In order to calculate the phasor polarization current density in time domain, we first multiply both side of Eq. (5.28) by $\omega^2 - j\omega\gamma_P$, we get

$$(\omega^2 - j\omega\gamma_P)\check{\mathbf{J}}_P = -j\omega\varepsilon_0\omega_P^2\check{\mathbf{E}} \tag{5.29}$$

then, we use the inverse Fourier Transformation on the frequency domain equation

$$\frac{\partial^2 \mathbf{J}_\mathrm{P}}{\partial t^2} + \gamma_P \frac{\partial \mathbf{J}_\mathrm{P}}{\partial t} = \varepsilon_0\omega_P^2 \frac{\partial \mathbf{E}}{\partial t} \tag{5.30}$$

Now, we integrate both side of Eq. (5.30)

$$\frac{\partial \mathbf{J}_\mathrm{P}}{\partial t} + \gamma_P \mathbf{J}_P = \varepsilon_0\omega_P^2\, \mathbf{E} \tag{5.31}$$

and then we perform the finite-difference to the partial differential terms,

$$\frac{\mathbf{J}_P^{n+1} - \mathbf{J}_P^n}{\Delta t} + \gamma_P \frac{\mathbf{J}_P^{n+1} + \mathbf{J}_P^n}{2} = \varepsilon_0\omega_P^2 \frac{\mathbf{E^{n+1}} + \mathbf{E^n}}{2} \tag{5.32}$$

$$\mathbf{J}_P^{n+1} = k_P\mathbf{J}_P^n + \zeta_P(\mathbf{E^{n+1}} + \mathbf{E^n}) \tag{5.33}$$

where,

$$k_P = \frac{2 - \gamma_P\Delta t}{2 + \gamma_P\Delta t} \tag{5.34}$$

and

$$\zeta_P = \frac{\varepsilon_0\omega_P^2\,\Delta t}{2 + \gamma_P\Delta t} \tag{5.35}$$

Since the Ampere's Law in Eq. (5.2), which is used to update the electric field, is centered at time $(n+\frac{1}{2})$, the polarization current density $\mathbf{J}$ must be represented at time $(n+\frac{1}{2})$. So, we apply a time-averaging for two terms at (n) and $(n+1)$

$$\mathbf{J}_P^{n+\frac{1}{2}} = \frac{1}{2}(\mathbf{J}_P^{n+1} + \mathbf{J}_P^{n}) = \frac{1}{2}[(1+k_P)\mathbf{J}_P^{n} + \zeta_P(\mathbf{E^{n+1}} + \mathbf{E^{n}})] \tag{5.36}$$

Then, the Ampere's Law takes the form

$$\begin{aligned}\nabla \times \mathbf{H}^{n+\frac{1}{2}} = \sigma\left(\frac{\mathbf{E}^{n+1}+\mathbf{E}^{n}}{2}\right) + \varepsilon_0\varepsilon_\infty\left(\frac{\mathbf{E}^{n+1}-\mathbf{E}^{n}}{\Delta t}\right) \\ + \frac{1}{2}\sum_{P=1}^{P}[(1+k_P)\mathbf{J}_P^{n} + \zeta_P(\mathbf{E^{n+1}} + \mathbf{E^{n}})]\end{aligned} \tag{5.37}$$

Thus, the update equation for electric field is

$$\begin{aligned}\mathbf{E}^{n+1} = \frac{2\varepsilon_0\varepsilon_\infty - \Delta t\sum_{P=1}^{P}\zeta_P - \sigma\Delta t}{2\varepsilon_0\varepsilon_\infty + \Delta t\sum_{P=1}^{P}\zeta_P + \sigma\Delta t}\mathbf{E}^{n} \\ + \frac{2\Delta t}{2\varepsilon_0\varepsilon_\infty + \Delta t\sum_{P=1}^{P}\zeta_P + \sigma\Delta t}\left\{\nabla \times \mathbf{H}^{n+\frac{1}{2}}\right. \\ \left. - \frac{1}{2}\sum_{P=1}^{P}(1+k_P)\mathbf{J}_P^{n}\right\}\end{aligned} \tag{5.38}$$

For dispersive material, the polarization current density $\mathbf{J}_P$ must be considered in the FDTD field update procedure.

5.5 Metamaterial as an Absorbed Material in the Proposed Structure

In this work, we will study the structure in Figure 4.1 with metamaterial as an absorbed material as shown in Figure 5.1. The FDTD method will be used to analyze the structure as in [70]. Metamaterial is purposed to improve the absorption of light. A slab of metamaterial effectively enhances evanescent waves that usually decay in other material and allow transmission of subwavelength to reach its maximum.

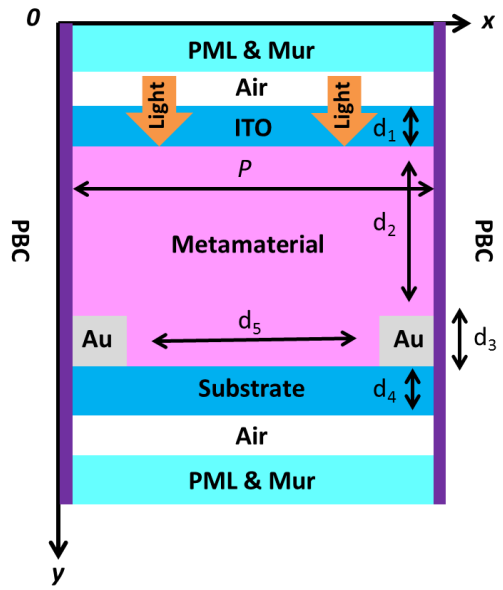

Figure 5.1 :The unit cell of the plasmonic thin-film solar cell [51].

5.5.1 The Auxiliary Differential Equation for Metamaterial

The time-dependent Maxwell's equations are,

$$\frac{\partial \mathbf{D}}{\partial t} = \nabla \times \mathbf{H} \tag{5.39}$$

$$\frac{\partial \mathbf{B}}{\partial t} = -\nabla \times \mathbf{E} \tag{5.40}$$

Since the cells of the domain are considered to have the same side, the electromagnetic field components are arranged on the cells as in the conventional FDTD method.

Now, using the central difference approximation for the time and space coordinates,

$$\frac{D_x^{n+\frac{1}{2}}(k) - D_x^{n-\frac{1}{2}}(k)}{\Delta t} = \frac{H_y^n(k+\frac{1}{2}) - H_y^n(k-\frac{1}{2})}{\Delta x} \tag{5.41}$$

$$\frac{B_y^n(k+\frac{1}{2}) - B_y^{n-1}(k+\frac{1}{2})}{\Delta t} = \frac{E_x^{n+\frac{1}{2}}(k) - E_x^{n+\frac{1}{2}}(k-1)}{\Delta x} \tag{5.42}$$

where, Δx is the space increment and Δt is the time step.

The above equations are used to update both the electric and magnetic field material with both positive permeability and permittivity. In case of metamaterial, the negative value of permeability and permittivity must be considered so,

$$D = \varepsilon(\omega) \times E \tag{5.43}$$

$$B = \mu(\omega) \times H \tag{5.44}$$

where, ε and μ are taken at a specific frequency in order to be negative. And they can be expressed as[80]

$$\varepsilon(\omega) = \varepsilon_0 \left(1 + \frac{\omega_{pe}^2}{\omega_{0e}^2 - \omega^2 + j\tau_e\omega}\right) \tag{5.45}$$

$$\mu(\omega) = \mu_0 \left(1 + \frac{\omega_{pm}^2}{\omega_{0m}^2 - \omega^2 + j\tau_m\omega}\right) \tag{5.46}$$

where, ε_0 and μ_0 are the free space permittivity and permeability, $\omega_{pe} = 2\pi f_{pe}$ and $\omega_{pm} = 2\pi f_{pm}$ are the electric and magnetic plasma frequency, ω_{0e} and ω_{0m} are the low frequency edge of electric and magnetic forbidden band, τ_e and τ_m are the electric and magnetic collision frequency.

In order to calculate the fields in the metamaterial layer, an Inverse Fourier Transform is used to change S-domain equations into time domain Auxiliary Differential Equations (ADE). Also, the central difference approximation method is used.

For metamaterial region, Eq. (5.43) becomes,

$$D(\omega) = \varepsilon_0 E(\omega) + \frac{\varepsilon_0 \omega_{pe}^2}{\omega_{0e}^2 - \omega^2 + j\tau_e\omega} E(\omega) \tag{5.47}$$

thus, the second term of Eq. (5.47) can be represented by a new parameter $S(\omega)$, where,

$$S(\omega) = \frac{\varepsilon_0 \omega_{pe}^2}{\omega_{0e}^2 - \omega^2 + j\tau_e\omega} E(\omega) \tag{5.48}$$

and Eq. (5.47) can be rewritten as,

$$D(\omega) = \varepsilon_0 E(\omega) + S(\omega) \tag{5.49}$$

Now, using $j\omega S(\omega) \leftrightarrow \frac{S^n - S^{n-2}}{2\Delta t}$ and $(j\omega)^2 S(\omega) \leftrightarrow \frac{S^n - 2S^{n-1} + S^{n-2}}{\Delta t^2}$, and denoting $S(\omega)$ as S^{n-1} in Eq. (5.48), the updated equation becomes,

$$\omega_{0e}^2 S^{n-1} + \frac{\tau_e (S^n - S^{n-2})}{2\Delta t} + \frac{S^n - 2S^{n-1} + S^{n-2}}{\Delta t^2} = \varepsilon_0 \omega_{pe}^2 E^{n-1} \qquad (5.50)$$

Hence, S^n can be calculated using the following equation,

$$S^n = \alpha\, S^{n-1} + \beta\, S^{n-2} + \gamma\, E^{n-1} \qquad (5.51)$$

where, $\alpha = \frac{2(2-\omega_{0e}^2 \Delta t^2)}{\tau_e \Delta t + 2}$, $\beta = \frac{\tau_e \Delta t - 2}{\tau_e \Delta t + 2}$ and $\gamma = \frac{2\Delta t^2 \omega_{pe}^2 \varepsilon_0}{\tau_e \Delta t + 2}$.

Thus, the updated equation of the electric field in the metamaterial layer in the time domain can be obtained by,

$$E^n = \frac{D^n - S^n}{\varepsilon_0} \qquad (5.52)$$

5.5.2 Results

For the two dimension thin film solar cell with periodic structure as shown in Figure 5.1, the absorbing material is metamaterial, the electrode is Au and the substrate is SiO_2, the geometric parameters of the proposed structure are set as d_1=25nm, d_2=120nm, d_3=40nm, d_4=30nm, d_5=100nm, and with a period of P=200nm. The y-directed incident field is the p-polarized plane wave with the amplitude of 1 and the frequency spectrum is from 400nm to 800nm. The spatial step is set to $\Delta_x = \Delta_y = 0.5$nm.

Figure 5.2 shows the Generalized Reflection Coefficients of the proposed solar cell structure with A-Si and metamaterial as an absorbed materials calculated by the FDTD method. It can be noticed that a strong optical absorption is observed from 550-640nm. The Generalized Reflection Coefficient reaches its minimum at 800nm for A-Si, and at 580nm for metamaterial.

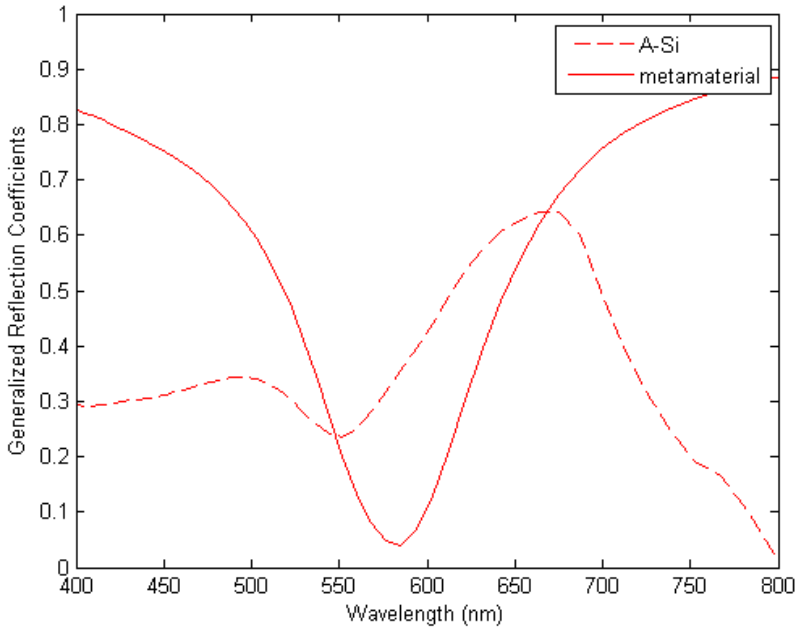

Figure 5.2 :The Generalized Reflection Coefficients for the proposed solar cell structure with A-Si and metamaterial as an absorbed materials calculated by the FDTD method.

Figure 5.3 shows the Reflection, Transmission and Loss in the proposed structure with metamaterial as an absorbed material. The Absorption reaches its maximum at 580nm which matches with the results of Figure 5.2.

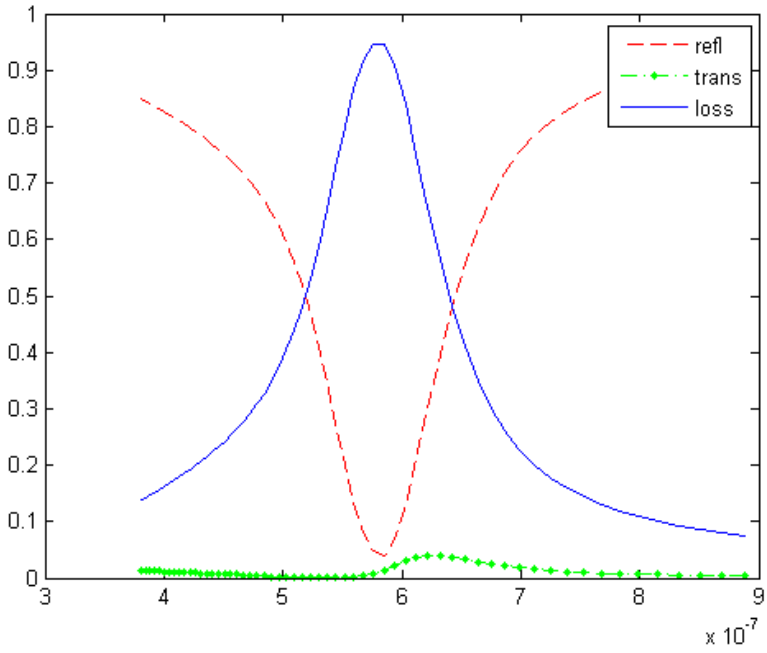

Figure 5.3: Reflection, Transmission and Loss in the proposed structure with metamaterial as an absorbed material.

5.6 Conclusions

In conclusion, a theoretical analysis based on FDTD has been introduced, discussed and implemented for newly waveguide structure containing Metamaterials for solar energy applications. The FDTD results have been confirmed and a strong optical absorption has been observed due to the Metamaterial layer.

Bibliography

1. Green, M.A., *Solar cells: operating principles, technology, and system applications.* 1982.
2. Nelson, J., *The physics of solar cells*. Vol. 57. 2003: World Scientific.
3. Würfel, P. and U. Würfel, *Physics of solar cells: from basic principles to advanced concepts*. 2009: John Wiley & Sons.
4. Polman, A. and H.A. Atwater, *Photonic design principles for ultrahigh-efficiency photovoltaics.* Nature materials, 2012. **11**(3): p. 174-177.
5. Reddy, P.J., *Science technology of photovoltaics*. 2010: BS publications.
6. Ayers, J.E., *Digital integrated circuits: analysis and design*. 2009: CRC Press, Inc.
7. Hashmi, M.H.I. and G. Shahida Rafique, *Towards high efficiency solar cells: composite metamaterials.* Global Journal of Researches In Engineering, 2013. **13**(10).
8. Carlson, D.E. and C. Wronski, *Amorphous silicon solar cell.* Applied Physics Letters, 1976. **28**(11): p. 671-673.
9. Bermel, P., et al., *Improving thin-film crystalline silicon solar cell efficiencies with photonic crystals.* Optics express, 2007. **15**(25): p. 16986-17000.
10. Shah, A., et al., *Thin-film silicon solar cell technology.* Progress in photovoltaics: Research and applications, 2004. **12**(2-3): p. 113-142.
11. Anderson, T., et al., *Fundamental materials research and advanced process development for thin-film CIS-based photovoltaics*. 2006, Technical Report NREL/SR-420-40568, National Renewable Energy Laboratory.
12. Nair, G. and M.G. Bawendi, *Carrier multiplication yields in CdSe and CdTe nanocrystals by transient photoluminescence.* arXiv preprint arXiv:0708.3866, 2007.
13. Grätzel, M., *Applied physics: solar cells to dye for.* Nature, 2003. **421**(6923): p. 586-587.
14. Nathan, S., et al. *Basic research needs for solar energy utilization*. in *Report on the basic energy sciences workshop on solar energy utilization. CIo Technology*. 2005.
15. Huynh, W.U., J.J. Dittmer, and A.P. Alivisatos, *Hybrid nanorod-polymer solar cells.* science, 2002. **295**(5564): p. 2425-2427.
16. Klimov, V., et al., *Optical gain and stimulated emission in nanocrystal quantum dots.* Science, 2000. **290**(5490): p. 314-317.
17. Yu, D., C. Wang, and P. Guyot-Sionnest, *n-Type conducting CdSe nanocrystal solids.* Science, 2003. **300**(5623): p. 1277-1280.
18. Liu, Y. and X. Zhang, *Metamaterials: a new frontier of science and technology.* Chemical Society Reviews, 2011. **40**(5): p. 2494-2507.
19. Hornby, A.S. and S. Wehmeier, *Oxford advanced learner's dictionary*. Vol. 1430. 1995: Oxford University Press Oxford.
20. Veselago, V.G., *THE ELECTRODYNAMICS OF SUBSTANCES WITH SIMULTANEOUSLY NEGATIVE VALUES OF IMG align= ABSMIDDLE alt= ϵ eps/IMG AND μ.* Physics-Uspekhi, 1968. **10**(4): p. 509-514.

21. Pendry, J., et al., *Low frequency plasmons in thin-wire structures.* Journal of Physics: Condensed Matter, 1998. **10**(22): p. 4785.
22. Pendry, J., et al., *Extremely low frequency plasmons in metallic mesostructures.* Physical review letters, 1996. **76**(25): p. 4773.
23. Smith, D.R., et al., *Composite medium with simultaneously negative permeability and permittivity.* Physical review letters, 2000. **84**(18): p. 4184.
24. Shelby, R.A., D.R. Smith, and S. Schultz, *Experimental verification of a negative index of refraction.* science, 2001. **292**(5514): p. 77-79.
25. Kong, J., *Electromagnetic wave interaction with stratified negative isotropic media.* Progress In Electromagnetics Research, 2002. **35**: p. 1-52.
26. Engheta, N., *Metamaterials with negative permittivity and permeability: background, salient features, and new trends.* Departmental Papers (ESE), 2003: p. 9.
27. Chew, W.C., *Some reflections on double negative materials.* Progress In Electromagnetics Research, 2005. **51**: p. 1-26.
28. Sabah, C., G. Ogucu, and S. Uckun, *Reflected and transmitted powers of electromagnetic wave through a double-negative slab.* Journal of Optoelectronics and Advanced Materials, 2006. **8**(5).
29. Sabah, C. and S. Uckun, *Electromagnetic wave propagation through frequency-dispersive and lossy double-negative slab.* Opto-Electronics Review, 2007. **15**(3): p. 133-143.
30. Mitchell, A.R. and D.F. Griffiths, *The finite difference method in partial differential equations*. 1980: John Wiley.
31. Kawano, K. and T. Kitoh, *Introduction to Optical Waveguide Analysis: Solving Maxwell's Equation and the Schrödinger Equation*. 2004: John Wiley & Sons.
32. Smith, G.D., *Numerical solution of partial differential equations: finite difference methods*. 1985: Oxford university press.
33. Sullivan, D.M., *Electromagnetic simulation using the FDTD method*. 2013: John Wiley & Sons.
34. Taflove, A. and S.C. Hagness, *Computational electrodynamics*. 2005: Artech house.
35. Yee, K.S., *Numerical solution of initial boundary value problems involving Maxwell's equations in isotropic media.* IEEE Trans. Antennas Propag, 1966. **14**(3): p. 302-307.
36. Engquist, B. and A. Majda, *Absorbing boundary conditions for numerical simulation of waves.* Proceedings of the National Academy of Sciences, 1977. **74**(5): p. 1765-1766.
37. Mur, G., *Absorbing boundary conditions for the finite-difference approximation of the time-domain electromagnetic-field equations.* Electromagnetic Compatibility, IEEE Transactions on, 1981(4): p. 377-382.
38. Berenger, J.-P., *Three-dimensional perfectly matched layer for the absorption of electromagnetic waves.* Journal of computational physics, 1996. **127**(2): p. 363-379.
39. Berenger, J.-P., *A perfectly matched layer for the absorption of electromagnetic waves.* Journal of computational physics, 1994. **114**(2): p. 185-200.

40. Chew, W., J. Jin, and E. Michielssen, *Complex coordinate stretching as a generalized absorbing boundary condition.* Microwave and Optical Technology Letters, 1997. **15**(6): p. 363-369.
41. Rappaport, C.M., M. Kilmer, and E. Miller, *Accuracy considerations in using the PML ABC with FDFD Helmholtz equation computation.* International Journal of Numerical Modelling: Electronic Networks, Devices and Fields, 2000. **13**(5): p. 471-482.
42. Hwang, J.-N., *A compact 2-D FDFD method for modeling microstrip structures with nonuniform grids and perfectly matched layer.* Microwave Theory and Techniques, IEEE Transactions on, 2005. **53**(2): p. 653-659.
43. Xu, F., et al., *Finite-difference frequency-domain algorithm for modeling guided-wave properties of substrate integrated waveguide.* Microwave Theory and Techniques, IEEE Transactions on, 2003. **51**(11): p. 2221-2227.
44. Luebbers, R., et al., *A frequency-dependent finite-difference time-domain formulation for dispersive materials.* Electromagnetic Compatibility, IEEE Transactions on, 1990. **32**(3): p. 222-227.
45. Zhao, Y.-J., K.-L. Wu, and K.-K.M. Cheng, *A compact 2-D full-wave finite-difference frequency-domain method for general guided wave structures.* Microwave Theory and Techniques, IEEE Transactions on, 2002. **50**(7): p. 1844-1848.
46. Thomas, J.W., *Numerical partial differential equations: finite difference methods*. Vol. 22. 2013: Springer Science & Business Media.
47. Zeng, L., et al., *Efficiency enhancement in Si solar cells by textured photonic crystal back reflector.* Applied Physics Letters, 2006. **89**(11): p. 111111.
48. Haase, C. and H. Stiebig, *Thin-film silicon solar cells with efficient periodic light trapping texture.* Applied Physics Letters, 2007. **91**(6): p. 061116.
49. Sai, H., et al., *Enhancement of light trapping in thin-film hydrogenated microcrystalline Si solar cells using back reflectors with self-ordered dimple pattern.* Applied Physics Letters, 2008. **93**(14): p. 143501.
50. Zhou, W., et al., *Microstructured surface design for omnidirectional antireflection coatings on solar cells.* Journal of Applied Physics, 2007. **102**(10): p. 103105.
51. Sha, W.E., W.C. Choy, and W.C. Chew, *A comprehensive study for the plasmonic thin-film solar cell with periodic structure.* Optics express, 2010. **18**(6): p. 5993-6007.
52. Barnes, W.L., A. Dereux, and T.W. Ebbesen, *Surface plasmon subwavelength optics.* Nature, 2003. **424**(6950): p. 824-830.
53. Zia, R., et al., *Geometries and materials for subwavelength surface plasmon modes.* JOSA A, 2004. **21**(12): p. 2442-2446.
54. Homola, J., S.S. Yee, and G. Gauglitz, *Surface plasmon resonance sensors: review.* Sensors and Actuators B: Chemical, 1999. **54**(1): p. 3-15.
55. Ditlbacher, H., et al., *Fluorescence imaging of surface plasmon fields.* Applied physics letters, 2002. **80**(3): p. 404-406.
56. Raether, H., *Surface plasmons on smooth surfaces*. 1988: Springer.

57. Kato, K., et al., *Enhancement of optical absorption and photocurrents in solar cells of merocyanine Langmuir–Blodgett films utilizing surface plasmon excitations.* Materials Science and Engineering: C, 2002. **22**(2): p. 251-256.
58. Tvingstedt, K., et al., *Surface plasmon increase absorption in polymer photovoltaic cells.* Applied Physics Letters, 2007. **91**(11): p. 113514.
59. Ferry, V.E., et al., *Plasmonic nanostructure design for efficient light coupling into solar cells.* Nano letters, 2008. **8**(12): p. 4391-4397.
60. Pala, R.A., et al., *Design of plasmonic thin-film solar cells with broadband absorption enhancements.* Advanced Materials, 2009. **21**(34): p. 3504-3509.
61. Qiu, M. and S. He, *A nonorthogonal finite-difference time-domain method for computing the band structure of a two-dimensional photonic crystal with dielectric and metallic inclusions.* Journal of applied physics, 2000. **87**(12): p. 8268-8275.
62. Farjadpour, A., et al., *Improving accuracy by subpixel smoothing in the finite-difference time domain.* Optics letters, 2006. **31**(20): p. 2972-2974.
63. Ong, K.G., et al., *Application of finite-difference time domain to dye-sensitized solar cells: The effect of nanotube-array negative electrode dimensions on light absorption.* Solar energy materials and solar cells, 2007. **91**(4): p. 250-257.
64. Chew, W.C., *Waves and fields in inhomogeneous media*. Vol. 522. 1995: IEEE press New York.
65. Chew, W.C. and W.H. Weedon, *A 3D perfectly matched medium from modified Maxwell's equations with stretched coordinates.* Microwave and optical technology letters, 1994. **7**(13): p. 599-604.
66. Oskooi, A.F., et al., *The failure of perfectly matched layers, and towards their redemption by adiabatic absorbers.* Optics Express, 2008. **16**(15): p. 11376-11392.
67. Palik, E.D., *Handbook of optical constants of solids*. Vol. 3. 1998: Academic press.
68. Chen, X.-W., W.C. Choy, and S. He, *Efficient and rigorous modeling of light emission in planar multilayer organic light-emitting diodes.* Journal of Display Technology, 2007. **3**(2): p. 110-117.
69. Musa, S.M., *Computational Nanotechnology Using Finite Difference Time Domain*. 2013: CRC Press.
70. Xiong, X.Y. and W. Sha, *The FDTD method: Essences, evolutions, and applications to nano-optics and quantum physics.* Computational Nanotechnology Using Finite Difference Time Domain, 2013. **2**: p. 37-82.
71. Sambles, J., G. Bradbery, and F. Yang, *Optical excitation of surface plasmons: an introduction.* Contemporary physics, 1991. **32**(3): p. 173-183.
72. Takayama, Y. and W. Klaus, *Reinterpretation of the auxiliary differential equation method for FDTD.* Microwave and Wireless Components Letters, IEEE, 2002. **12**(3): p. 102-104.
73. Jiong, S., *Auxiliary equation method for solving nonlinear partial differential equations.* Physics Letters A, 2003. **309**(5): p. 387-396.
74. Ziolkowski, R.W. and M. Tanaka, *Finite-difference time-domain modeling of dispersive-material photonic bandgap structures.* JOSA A, 1999. **16**(4): p. 930-940.

75. Taflove, A. and S.C. Hagness, *Computational electrodynamics: the finite-difference time-domain method.* Norwood, 2nd Edition, MA: Artech House, l995, 1995.
76. Alsunaidi, M. and A. Al-Jabr, *A general ADE-FDTD algorithm for the simulation of dispersive structures.* Photonics Technology Letters, IEEE, 2009. **21**(12): p. 817-819.
77. Kong, S.-C., J.J. Simpson, and V. Backman, *ADE-FDTD scattered-field formulation for dispersive materials.* Microwave and Wireless Components Letters, IEEE, 2008. **18**(1): p. 4-6.
78. Pernice, W., F. Payne, and D. Gallagher, *An FDTD method for the simulation of dispersive metallic structures.* Optical and quantum electronics, 2006. **38**(9-11): p. 843-856.
79. Lee, K.H., et al., *Implementation of the FDTD method based on Lorentz-Drude dispersive model on GPU for plasmonics applications.* Progress In Electromagnetics Research, 2011. **116**: p. 441-456.
80. Furse, C.M., J.-Y. Chen, and O.P. Gandhi, *The use of the frequency-dependent finite-difference time-domain method for induced current and SAR calculations for a heterogeneous model of the human body.* Electromagnetic Compatibility, IEEE Transactions on, 1994. **36**(2): p. 128-133.